Retinal defects in mice lacking the autism-associated gene *Engrailed-2*

Xuwen Zhang[1], Ilaria Piano[2], Andrea Messina[3], Vanessa D'Antongiovanni[4], Fabiana Crò[1]*, Giovanni Provenzano[1], Yuri Bozzi[3,5], Claudia Gargini[2], Simona Casarosa[1,5]

[1] Centre for Integrative Biology, University of Trento, Trento, Italy

[2] Department of Pharmacy, University of Pisa, Pisa, Italy

[3] Center for Mind/Brain Sciences (CIMeC), University of Trento, Rovereto, Italy

[4] Department of Clinical and Experimental Medicine, University of Pisa, Italy.

[5] CNR Neuroscience Institute, Pisa, Italy

*present address: Gruppo SYNLAB Italia, Castenedolo, Lombardia, Italia

Correspondence should be addressed to:

Prof. Simona Casarosa,
Laboratory of Neural Development and Regeneration
Centre for Integrative Biology (CIBIO)
Via Sommarive 9, 38123 Trento, Italy
email: simona.casarosa@unitn.it

Prof. Yuri Bozzi,
Neurodevelopmental Disorders Research Group
Center for Mind/Brain Sciences (CIMeC), University of Trentoi
Corso Bettini 31, Rovereto (TN), Italy
email: yuri.bozzi@unitn.it

Abstract

Defective cortical processing of visual stimuli and altered retinal function have been described in autism spectrum disorder (ASD) patients. In keeping with these findings, anatomical and functional defects have been found in the visual cortex and retina of mice bearing mutations for ASD-associated genes. Here we sought to investigate the anatomy and function of the adult retina of *Engrailed 2* knockout *(En2$^{-/-}$)* mice, a model for ASD. Our results showed that *En2* is expressed in all three nuclear layers of the adult retina. When compared to age-matched *En2$^{+/+}$* controls, *En2$^{-/-}$* adult retinas showed a significant decrease in the number of calbindin^{+} horizontal cells, and a significant increase in calbindin^{+} amacrine/ganglion cells. The total number of ganglion cells was not altered in the adult *En2$^{-/-}$* retina, as shown by *Brn3a^{+}* cell counts. In addition, *En2$^{-/-}$* adult mice showed a significant reduction of photoreceptor (rhodopsin) and bipolar cell (*Pcp2,* PKCα) markers. Functional defects were also present in the retina of *En2* mutants, as indicated by electroretinogram recordings showing a significant reduction in both a-wave and b-wave amplitude in *En2$^{-/-}$* mice as compared to controls. These data show for the first time that anatomical and functional defects are present in the retina of the *En2* ASD mouse model.

KEYWORDS

Retina, electroretinogram, neurodevelopmental disorder, vision, photoreceptor.

ABBREVIATIONS

ASD, autism spectrum disorders

BSA, bovine serum albumin

En2, Engrailed-2

ERG, electroretinogram

GABA, γ-aminobutyric acid

GAPDH, glyceraldehyde 3-phosphate dehydrogenase

GCL, ganglion cell layer

IB, immunoblotting

IHC, immunohistochemistry

INL, inner nuclear layer

ONL, outer nuclear layer

OP, oscillatory potential

OS, outer segment

PFA, paraformaldehyde

PKCα, protein kinase Cα

PSD-95, postsynaptic density protein 95

qRT-PCR, quantitative reverse transcription PCR

Rho, rhodopsin

ROS, rod outer segment

SDS-PAGE, sodium-dodecyl-sulphate polyacrylamide gel electrophoresis

VEP, visual evoked potentials

Introduction

The *Engrailed-2* (*En2*) gene is a homeobox-containing transcription factor, involved in the regionalization, patterning and neural differentiation of the midbrain/hindbrain region (Joyner et al., 1991; Joyner, 1996). *En2* is widely expressed in the midbrain/hindbrain region (including the cerebellum primordium), starting at embryonic day 8.5 and continuing throughout embryonic and postnatal development (Joyner 1996; Gherbassi and Simon, 2006). *En2* mRNA is also expressed in the hippocampus and cerebral cortex of adult mouse (Tripathi et al., 2009; Sgadò et al., 2013). Mice lacking the homeobox-containing transcription factor *En2* (*En2*$^{-/-}$) are a reliable model for investigating the neurodevelopmental basis of autism spectrum disorders (ASD). Genetic studies (Gharani et al., 2004; Benayed et al., 2005, 2009; Hnoonual et al., 2016) and expression analyses on post-mortem brain tissues (James et al., 2013, 2014; Choi et al., 2014) showed that deregulated expression of the human EN2 gene is linked to ASD.

En2$^{-/-}$ mice display ASD-like behaviors (Cheh et al., 2006; Brielmaier et al., 2012; Provenzano et al., 2014) accompanied by ASD-relevant anatomical deficits, including cerebellar hypoplasia (Joyner et al., 1991; Kuemerle et al., 1997) and loss of GABAergic interneurons in somatosensory (Sgadò et al., 2013) and visual cortical (Allegra et al., 2014) areas. Interneuron defects in the *En2*$^{-/-}$ visual cortex are accompanied by altered binocularity and reduced visual cortical plasticity, while visual functional properties (acuity, response latency, receptive field size) are unaffected in *En2*$^{-/-}$ mutant mice (Allegra et al., 2014).

Sensory processing has been given an increasing attention in both ASD diagnosis and research in recent years (Robertson and Baron-Cohen, 2017). Enhanced visual evoked potentials (VEP) responses to high spatial frequencies were found in visual brain areas of ASD children, while unaffected control children

generally responded to visual stimuli with low spatial frequency (Vlamings et al., 2010). This is in agreement with previous studies showing that visual perception in ASD is more detail-oriented, suggesting that primary visual processing might also contribute to social and communication deficits in ASD (Dakin and Frith, 2005; Happé and Frith, 2006; Mottron et al., 2006; Behrmann et al., 2006). In addition, defective retinal function has been described in human ASD patients (Lavoie et al., 2014; Constable et al., 2016).

In keeping with these findings, anatomical and functional defects were found in the retina of *Fmr1* knockout mice (Rossignol et al., 2014), a syndromic ASD model sharing neuroanatomical (Ellegood et al., 2015) and molecular (Provenzano et al., 2015) abnormalities with *En2*$^{-/-}$ mice. To understand whether retinal defects are a common neuropathological feature in ASD mouse models, here we sought to investigate the morphology and function of the *En2*$^{-/-}$ adult retina.

EXPERIMENTAL PROCEDURES

Animals. All experimental procedures were performed in accordance with the European Communities Council Directive 2010/63/EU and were approved by the Animal Welfare Committee of the University of Trento and the Italian Ministry of Health. Animals were housed in a 12h light/dark cycle with food and water available *ad libitum,* and all efforts were made to minimize animals' suffering during experimental procedures. The original *En2* mutant strain (mixed 129Sv × C57BL/6 genetic background; Joyner et al., 1991) was backcrossed at least five times into a C57BL/6 background (Sgadò et al., 2013). Heterozygous matings ($En2^{+/-}$ × $En2^{+/-}$) were used to obtain $En2^{+/+}$ and $En2^{-/-}$ littermates used in this study. Mice were genotyped according to published protocols (www.jax.org; mouse strain $En2^{tm1Alj}$). All experiments were performed on adult animals (3-5 months old; weight = 25-35 g) of both sexes, since previous studies showed that behavioral traits and gene expression profiles did not differ between genders in both $En2^{+/+}$ and $En2^{-/-}$ mice (Brielmaier et al., 2012; Sgadò et al., 2013). A total of 66 mice were used in this study. Twelve mice (6 per genotype) were used for quantitative reverse transcription PCR (qRT-PCR) and laser-capture microdissection, 6 (3 per genotype) for *in situ* hybridization, 8 (4 per genotype) for immunohistochemistry on retinal sections, 22 (11 per genotype) for whole-mount immunohistochemistry, 6 (3 per genotype) immunoblotting, and 12 (6 per genotype) for electroretinogram (ERG). For anatomy and gene expression experiments, eyes were rapidly removed after cervical dislocation. For ERG, mice received 20% urethane (0.1ml/10g of body weight) and were sacrificed at the end of the experiment by cervical dislocation without awakening from anesthesia.

Laser-capture microdissection. Eyes from adult *En2*$^{+/+}$ mice were embedded in Tissue-Tek O.C.T. compound (Sakura-VWR), frozen on dry ice, and stored at -80°C. Frozen tissues were cut into 12 µm thick sections and collected on RNase-free polyethylene naphthalate membrane slides (Leica). Sections were then thawed and fixed in 75% ethanol for 30s, counterstained with hematoxylin and eosin for 45 s, and washed in RNase-free water for 30 s. Finally, the sections were dehydrated in graded ethanol and air-dried. Three retinal layers (ganglion cell layer, inner nuclear layer, and outer nuclear layer) were dissected on a laser capture microdissection (LCM) system (LMD6500, Leica). Total RNA was extracted from the captured layers by using the PicoPure RNA Isolation Kit (Life Technologies). On-column digestion with RNase-Free DNase Set (Qiagen) was performed to ensure the removal of possible genomic DNA contamination. Samples were reversed transcribed and subjected to qRT-PCR analysis.

In situ hybridization. Eyes from *En2*$^{+/+}$ and *En2*$^{-/-}$ mice were rapidly removed and fixed by immersion in 4% PFA after removal of the cornea and lens. After fixation, the eyecups were cryoprotected in 20% sucrose, embedded in Tissue-Tek O.C.T. compound (Sakura-VWR), and 12 µm thick cryostat sections were serially cut (Leica CM1850). Non-radioactive *in situ* hybridization was performed as previously described (Tripathi et al., 2009) using a digoxigenin-labeled *En2* riboprobe (Genbank ID: NM_010134). The *En2* antisense riboprobe was generated from a T3 RNA polymerase promoter flanking a cDNA fragment of approximately 440 base pairs generated by RT-PCR from cerebellar RNA. Primers used for *in situ* hybridization are listed in Table 1. Signal was detected by alkaline phosphatase–conjugated anti-digoxigenin antibody followed by alkaline phosphatase staining. Stained sections

were photographed using an AxioCam MRm camera connected to a Zeiss Axio Imager M2 microscope (Carl Zeiss).

qRT-PCR. Total RNAs from *En2*$^{+/+}$ and *En2*$^{-/-}$ mice eyes were extracted by Nucleospin RNA XS kit (Macherey-Nagel). cDNA was synthesized from the total RNAs (1µg) by SuperScript VILO cDNA Synthesis Kit (Invitrogen). qRT-PCR was performed in a C1000 Thermal Cycler (Bio-Rad) with real-time detection of fluorescence, using the KAPA SYBR FAST Master Mix reagent (KAPA Biosystems). Mouse beta-actin (β-actin) was used as an internal standard for quantification analysis. Primers used for qRT-PCR are reported in Table 1. Ratios of comparative concentrations of each mRNA with respect to β-actin mRNA were then calculated and plotted as the average of three independent reactions with technical replicates obtained from each RNA sample. Expression analysis was performed using the CFX3 Manager (BioRad) software.

Immunohistochemistry. Eyes from *En2*$^{+/+}$ and *En2*$^{-/-}$ mice were rapidly removed and fixed by immersion in 4% paraformaldehyde (PFA) after removal of the cornea and lens. For immunohistochemistry on whole-mounted retinas, retinas were crosscut in 1x PBS to flatten them. For immunohistochemistry on sections, eyecups were cryoprotected in 20% sucrose, embedded in Tissue-Tek O.C.T. compound (Sakura-VWR), and serially cut (12 µm thick) at the cryostat (Leica CM1850).

Immunohistochemistry was performed as follows: whole-mounted retinas were incubated in blocking solution containing 0.3% Triton X-100 and 5% BSA in 1x PBS overnight at 4°C followed by 3 days of incubation in 0.1% Triton X-100 and 1% BSA in 1×PBS at 4°C in a stable agitator, with the primary antibody. Cryostat sections

were blocked in blocking solution containing 0.5% Triton X-100, 1% BSA and 10% fetal bovine serum in 1x PBS at room temperature for 1hr followed by overnight incubation at 4°C with 0.5% Triton X-100, 1% BSA, and 3% FBS in 1x PBS, with primary antibodies. Samples were then incubated 2 days (flat-mounts at 4°C) or 2hrs (sections at room temperature) with secondary antibodies conjugated to either Alexa 488 or Alexa 594, washed in 1x PBS and mounted onto glass slides using Aqua-Poly/Mount coverslipping medium (Polysciences, Inc.). Primary and secondary antibodies used are listed in Table 2.

***Image acquisition and cell counting*.** Image stacks were acquired using a Zeiss Axio Observer Z1 microscope (Zeiss) equipped with Axiocam 503 mono camera. Full mosaic images of whole mount retina tissues were acquired by the tile function of the microscope using an EC Plan-Neofluar 20x or 40x objective for the quantitative analysis of calbindin$^+$ horizontal/amacrine/ganglion cells or Brn-3a$^+$ ganglion cells. Z-plane, exposure time and microscope settings were optimized for each marker and cell type, and then kept constant in all acqisitions for both genotypes. For cell counting, 8 tile images in the central part of each wing of the retina were extracted, therefore a total of 32 tile images were extracted per retina per genotype to count cells. Cell counting was performed by Columbus software (PerkinElmer) or Image J software (NIH) in a consistent way. Parameters (common threshold, area, split factor, individual threshold, contrast, cell roundness) for defining and selecting the objective cells were optimized for each marker using the Columbus software. All the images for each specific marker, from both genotypes, were analyzed under the same set of parameters in the Columbus software. Cell counting for calbindin$^+$ amacrine/ganglion cells was performed manually by using Image J. Cell densities were then plotted as the total number of positive cells in total counting area.

Immunoblotting. Total proteins were extracted from *En2*$^{+/+}$ and *En2*$^{-/-}$ eyes using a standard protocol, under reducing conditions. Total protein extracts were separated by standard SDS-PAGE, blotted and incubated with the different antibodies, as indicated in Table 2. Immunoblots were revealed and quantified using chemiluminescence followed by densitometry using Image J (NIH). GAPDH was used as an internal standard for protein quantification analysis.

Electroretinogram (ERG) recordings. ERGs were recorded from dark-adapted mice by means of coiled gold electrodes making contact with the cornea moisturized by a thin layer of gel. Pupils were fully dilated by application of a drop of 1% atropine (Farmigea, Pisa, Italy). Scotopic ERG recordings were average responses (n = 5) to flashes of increasing intensity (1.7×10^{-5} to 377.2 cd*s/m^2, 0.6 log units steps) presented with an inter-stimulus interval ranging from 20 s for dim flashes to 1 min for the brightest flashes. Isolated cone (photopic) components were obtained by superimposing the test flashes (0.016 to 377.2 cd*s/m^2, 0.6 log units steps) on a steady background of saturating intensity for rods (30 cd/m^2), after at least 15 min from background onset. Amplitude of the a-wave was measured at 7 ms after the onset of light stimulus and the b-wave was measured from the peak of the a-wave to the peak of the b-wave. Oscillatory potentials (OPs) were also measured in both scotopic and photopic conditions. OPs were extracted digitally by using a fifth-order Butterworth filter as previously described (Hancock et al., 2004; Lei et al., 2006). Peak amplitude of each OP (OP1–OP4) was measured. ERG data for each condition of light-induction were collected from 6 animals per genotype.

Statistical analyses. Statistical analysis was performed by Prism 6 software (GraphPad). qRT-PCR, immunoblotting and immunohistochemistry data were analysed with a non-parametric (Mann-Whitney U) test (*En2*$^{+/+}$ vs. *En2*$^{-/-}$). ERG data were analysed by two-way ANOVA (factors: genotype and flash intensity) followed by post-hoc Tuckey test for multiple comparisons. Values of b-wave/a-wave ratio of scotopic ERG were analysed by Student's t-test. In all tests, statistical significance level was set at $p<0.05$.

RESULTS

***En2 is expressed in adult mouse retina*.** We first investigated whether *En2* is expressed in the adult mouse retina. To this aim, we performed RT-PCR on RNAs extracted from whole retinas and from the three retinal nuclear layers obtained by laser-capture microdissection. RT-PCR showed that *En2* mRNA was expressed in the retina of $En2^{+/+}$ but not $En2^{-/-}$ adult mice (Fig. 1A). *Engrailed 1* (*En1*) mRNA, whose expression largely overlaps with that of *En2* (Joyner, 1996), was not detected in the retina of $En2^{+/+}$ nor $En2^{-/-}$ adult mice (data not shown). *En2* mRNA was localized in all three nuclear layers (Fig. 1B), as confirmed by *in situ* hybridization (Fig. 1C). Immunohistochemistry with an En2-specific antibody revealed that En2 nuclear staining was localized in the inner nuclear (INL) and ganglion cell (GCL) layers, but not in the photoreceptor cell (outer nuclear, ONL) layer (Figure 1D).

Rhodopsin expression is downregulated in the $En2^{-/-}$ adult retina. Since *En2* is expressed in all three nuclear layers of the adult mice retina, we asked whether retinal neurons are affected in the absence of *En2*. We first characterized rod photoreceptors, which account for the majority of photoreceptors in the mouse retina [Jeon et al., 1998; Haverkamp and Wässle, 2000]. We first performed immunohistochemistry on $En2^{+/+}$ and $En2^{-/-}$ retinal sections using the rod photoreceptor specific marker rhodopsin, which labels the rod outer segment (ROS) disk membrane. Rhodopsin immunohistochemistry did not show significant differences between $En2^{-/-}$ and $En2^{+/+}$ ROS (Fig. 2A). qRT-PCR analysis showed a significant downregulation of rhodopsin mRNA in the $En2^{-/-}$ retina ($p<0.05$, Mann-Whitney U test, $En2^{+/+}$ vs. $En2^{-/-}$; n=3 per genotype; Fig. 2B). In keeping with these findings, immunoblotting experiments showed that the rhodopsin dimer isoform (78 kDa) was significantly downregulated in the $En2^{-/-}$ mice retina, as compared to $En2^{+/+}$

controls ($p<0.01$, Mann-Whitney U test, *En2*$^{+/+}$ vs. *En2*$^{-/-}$; n=3 per genotype; Fig. 2C). Levels of rhodopsin oligomer (114 kDa, Fig. 2C) and monomer (40 kDa, not shown) isoforms did not differ between genotypes.

Cone photoreceptor markers are unchanged in the En2$^{-/-}$ adult retina. We next investigated the expression of cone photoreceptor markers in *En2*$^{+/+}$ and *En2*$^{-/-}$ adult retinas. Immunohistochemistry for the cone photoreceptor marker cone-arrestin showed that the structure of the outer segment (OS) of cone photoreceptors is comparable between *En2*$^{-/-}$ and *En2*$^{+/+}$ mice (Fig. 3A). In the mouse retina, there are two subtypes of cone photoreceptors: short-wavelength (blue) sensitive cones (S-cones) and medium-wavelength (green/red) sensitive cones (M-cones), which express different types of opsins (S opsin and M opsin, respectively). qRT-PCR showed comparable levels of S opsin and M opsin mRNAs in adult *En2*$^{+/+}$ and *En2*$^{-/-}$ retinas ($p>0.05$, Mann-Whitney U test, *En2*$^{+/+}$ vs. *En2*$^{-/-}$, 3 mice per genotype; Fig. 3B). Similarly, immunoblotting experiments did not reveal any significant changes of S and M opsin protein levels between the two genotypes ($p>0.05$, Mann-Whitney U test, *En2*$^{+/+}$ vs. *En2*$^{-/-}$; n=3 per genotype; Fig. 3C). Finally, to understand whether photoreceptor synaptic terminals were altered in the *En2*$^{-/-}$ mice retina, we performed immunohistochemistry for postsynaptic density protein 95 (PSD- 95), which strongly labels the excitatory axon terminals of rods and cones in the outer plexiform layer (Koulen et al., 1998). PSD-95 labelled photoreceptor synaptic terminals showed no difference between *En2*$^{+/+}$ and *En2*$^{-/-}$ mice (Fig. 3D).

Altered expression of bipolar cell markers in the En2$^{-/-}$ adult retina. Photoreceptor cells transmit their signals to bipolar cells. To characterize bipolar cells, we first performed qRT-PCR for the specific marker Purkinje cell protein 2

(*Pcp2*; Xu et al., 2008). *Pcp2* mRNA showed a significant reduction in the *En2*$^{-/-}$ adult retina, as compared to age-matched *En2*$^{+/+}$ controls ($p<0.001$, Mann-Whitney U test, *En2*$^{+/+}$ vs. *En2*$^{-/-}$, 3 mice per genotype; Fig. 4A). Immunohistochemistry for the bipolar cells marker protein kinase Cα (PKCα Haverkamp et al., 2003) did not reveal significant differences between *En2*$^{-/-}$ and *En2*$^{+/+}$ adult retinas (Fig. 4B).

Decreased density of calbindin^{+} horizontal cells in the En2$^{-/-}$ adult mouse retina. In the mouse retina, horizontal cells laterally interconnect with photoreceptors and bipolar cells. To characterize these cells, we performed whole-mount immunohistochemistry experiments on *En2*$^{+/+}$ vs. *En2*$^{-/-}$ retinas using the specific marker calbindin (Mitchell et al., 1995). Calbindin^{+} horizontal cell density was significantly reduced in the *En2*$^{-/-}$ adult retina, as compared to *En2*$^{+/+}$ controls (Fig. 5A). Quantification of cell counts confirmed these findings ($p<0.05$, Mann-Whitney U test, n=4 mice per genotype; Fig. 5B).

Increased density of calbindin^{+} amacrine and ganglion cells in the En2$^{-/-}$ adult mouse retina. In the mouse retina, calbindin is known to stain also amacrine cells in the inner part of the INL, ganglion cells, and displaced amacrine cells in the GCL. We therefore selectively acquired calbindin immunofluorescence in the INL/GCL of *En2*$^{+/+}$ and *En2*$^{-/-}$ mice whole retinas (Fig. 5B). Quantification of cell counts showed a statistically significant increase of calbindin^{+} amacrine/ganglion cell density in *En2*$^{-/-}$ retina, as compared to aged-matched *En2*$^{+/+}$ controls ($p<0.05$, Mann-Whitney U, n=4 mice per genotype; Fig. 5D). In keeping with these findings, qRT-PCR experiments showed significantly increased mRNA levels of the GABAergic amacrine marker parvalbumin in the *En2*$^{-/-}$ retina, as compared to *En2*$^{+/+}$ controls ($p<0.01$, Mann-Whitney U test, *En2*$^{+/+}$ vs. *En2*$^{-/-}$, 3 mice per genotype; Fig. 6). We finally investigated

retinal ganglion cell density by brain-specific homeobox/POU domain protein 3a (Brn3a) immunohistochemistry on *En2*$^{+/+}$ and *En2*$^{-/-}$ whole-mounted retinas (Fig. 5E), which revealed no significant difference between the two genotypes ($p>0.05$, Mann-Whitney U test, *En2*$^{+/+}$ vs. *En2*$^{-/-}$, 3 mice per genotype; Fig. 5F).

Impairment of scotopic retinal function in En2*$^{-/-}$ *mice. Retinal function was evaluated by both scotopic and photopic ERG recordings. *En2*$^{-/-}$ mice showed a reduction in scotopic ERG response, as compared to *En2*$^{+/+}$ age-matched controls (Fig. 7A). The amplitude of the 7ms a-wave, which represents the inhibition of rod dark-current, showed a significant reduction in *En2*$^{-/-}$ animals as compared to *En2*$^{+/+}$ (two-way ANOVA; main effect of genotype $F_{(1,84)}=6.796$, $p = 0.012$; main effect of flash intensity $F_{(1,84)}=15.748$, $p<0.001$; Tukey's test following two-way ANOVA; *En2*$^{+/+}$ vs. *En2*$^{-/-}$ at 377.2 cd*s/m^2, $p<0.01$; n=6 per genotype; Fig. 7B). The b-wave amplitude was also significantly reduced in *En2*$^{-/-}$ mice, as compared to *En2*$^{+/+}$ controls (two-way ANOVA; main effect of genotype $F_{(1,144)}=41.187$, $p<0.001$; main effect of flash intensity $F_{(1,144)}=25.434$, $p=0$; Tukey's test following two-way ANOVA, *En2*$^{+/+}$ vs. *En2*$^{-/-}$ $p<0.01$ at 377.2 and 83.7 cd*s/m^2, $p<0.05$ at flash intensity level between 1.29 and 21.2 cd*s/m^2; n=6 per genotype; Fig. 7C). In order to investigate where the functional changes originate, we analyzed the b-wave/a-wave ratio of scotopic ERG (Piano et al., 2016). This ratio, measured at maximal flash intensity (377.2 cd*s/m^2), was comparable in *En2*$^{+/+}$ and *En2*$^{-/-}$ mice (*En2*$^{+/+}$, 7.71±1.58; *En2*$^{-/-}$, 8.51±1.0; $p>0.05$, Student's *t*-test, *En2*$^{+/+}$ vs. *En2*$^{-/-}$; n=6 per genotype). This suggests that the reduction of b-wave amplitude observed in *En2*$^{-/-}$ mice directly depends on the reduction of the a-wave amplitude, indicating a defect in rod photoreceptors in mutant mice. Conversely, the kinetics of the response (Fig. 7D) and scotopic OPs amplitude (Fig. 7E) did not differ between *En2*$^{-/-}$ and *En2*$^{+/+}$ mice. No difference

between the two genotypes was found when evaluating the scotopic peak time (kinetic response; Fig. 7F).

Preservation of photopic retinal function in En2$^{-/-}$ mice. Figure 8 shows the results obtained from the photopic ERG recordings. The amplitude of the photopic b-wave showed no difference between *En2*$^{-/-}$ and *En2*$^{+/+}$ mice, and also the kinetics was completely superimposable between the two genotypes. The analysis of OPs also showed no difference between *En2*$^{-/-}$ and *En2*$^{+/+}$ mice.

DISCUSSION

Brief summary of results

In this study, we showed that the ASD-associated gene *En2* is expressed in all three nuclear layers of the adult retina. Immunohistochemical analyses showed a significantly reduced expression of photoreceptor and bipolar cell markers in *En2*$^{-/-}$ retinas, accompanied by a significantly altered number of calbindin^{+} horizontal and amacrine/ganglion cells (Table 3). ERG recordings showed a significant reduction in scotopic a-wave and b-wave amplitude in *En2*$^{-/-}$ mice, as compared to controls. These data show for the first time that anatomical and functional defects are present in the retina of the *En2* mutant mice.

En2 is expressed in the adult mouse retina

Previous studies showed from our and other laboratories clearly showed that *En2* mRNA, in addition to being expressed in the developing mesencephalon and cerebellum, is also detected in several areas of the postnatal forebrain, including the hippocampus and neocortex (Tripathi et al., 2009; Brielmaier J., 2012; Sgadò et al, 2013; Allegra et al., 2014; Provenzano et al., 2014; Soltani et al., 2018). The present study confirms that *En2* is expressed in anterior regions of the central nervous system. Our data show that *En2* mRNA is present in all nuclear layers of the adult mouse retina, while En2 protein nuclear staining is detected in INL and GCL but not in the photoreceptor layer. A previous study reported a selective *En2* mRNA expression in cone photoreceptors (Siegert et al., 2012), and more recent RNA sequencing datasets showed minimal or no expression of *En2* in purified rod photoreceptors (Kim et al., 2016; Mo et al., 2016; Hughes et al., 2017). Our non-quantitative RT-PCR data from laser-capture microdissected retinal layers do not allow us to identify the cell types expressing En2 mRNA. Moreover, it should also be

considered that *En2* mRNA signal could result from Müller glia cells, whose cell bodies are present in all three retinal cell layers. Thus, our *in situ* hybridization data showing *En2* mRNA expression in the photoreceptor layer should be interpreted with extreme caution. Expression of En2 in the INL/GCL was instead corroborated by immunostaining, suggesting that the En2 protein is present in amacrine and possibly ganglion cells (Fig. 1D).

_En2_ inactivation alters rod photoreceptor and bipolar cell marker expression

The expression profile of *En2* in the adult retina led us to investigate whether *En2* gene inactivation resulted in retinal structural and/or functional defects. We first observed a significant down-regulation of the rod photoreceptor-specific marker rhodopsin the *En2*$^{-/-}$ retina, at both mRNA and protein level (Fig. 2). Cone photoreceptor markers were instead unchanged in the *En2*$^{-/-}$ retina (Fig. 3). The reduction of rhodopsin might be caused by the loss of *En2* transcriptional regulation, as a similar effect was observed in the absence of other homeobox transcription factors. As an example, mice lacking *Crx,* a photoreceptor-specific transcription factor, show a disrupted morphogenesis of the photoreceptor outer segment, and fail to produce the phototransduction apparatus (Furukawa et al., 1997). En2, as Crx, binds the DNA sequence TAATTC/A (Ades and Sauer, 1994), which is found upstream of several photoreceptor-specific genes (Freund et al., 1997), and this might explain the altered expression of photoreceptor markers observed in *En2*$^{-/-}$ mice. However, it remains to be investigated how the loss of En2, which is virtually absent from rod photoreceptors (Kim et al., 2016; Mo et al., 2016; Hughes et al., 2017; and see also Fig. 1D), might result in rod phototransduction defects. Previous work showed that a gradient of Engrailed proteins secreted by tectal neurons is able to guide retinal axon growth in a topographical manner (Brunet et al., 2005;

Wizenmann et al., 2009). Although secretion of Engrailed proteins by retinal cells has not been shown so far (Wizenmann et al., 2015), in principle we can not exclude that En2 expressed in the INL (Figure 1) and secreted by INL neurons can act on other retinal cell types.

Bipolar cell markers were also affected in the *En2*$^{-/-}$ retina. Our results showed a significant reduction of the mRNA for the bipolar cell marker *Pcp2*, as compared to age-matched controls; *En2*$^{-/-}$ bipolar cells also showed shorter axons, as revealed by PKCα immunohistochemistry (Fig. 4). This suggests the absence of the *En2* transcription factor also impacts on the transcriptomic profile of rod bipolar cells, which express *Pcp2* (Xu et al., 2008) and PKCα (Haverkamp et al., 2003). It is however important to point out that in this study we did not count the number of photoreceptors and bipolar cells. Therefore, it remains unclear whether the observed physiological defects arise from changes in gene expression of the investigated markers, or in the numbers of these cell subtypes.

Altered cells density of horizontal and amacrine cells in the *En2*$^{-/-}$ retina

Horizontal cells modulate the lateral signal transmission neurotransmission between the photoreceptors and bipolar cells. Negative feedback from horizontal cells to cones and direct feed-forward input from horizontal cells to bipolar cells are responsible for generating center-surround receptive fields that enhance spatial discrimination (Thoreson and Mangel, 2012). Our results a significant reduction of calbindin^{+} horizontal cells in the *En2*$^{-/-}$ retina (Fig. 5A, B). Mice lacking horizontal cells show multiple functional defects, such as altered firing properties and receptive field formation of retinal ganglion cells, impaired ambient light adaptation, and altered optokinetic responses (i.e., reflexive eye movements elicited by a moving visual pattern) (Chaya et al., 2017). Thus, partial loss of horizontal cells in the *En2*$^{-/-}$ retina

might affect several different aspects of visual processing; further studies are needed to elucidate the impact of reduced horizontal cell density in *En2*$^{-/-}$ mice.

Amacrine cell density was instead increased in the *En2*$^{-/-}$ retina (Fig. 5C, D); accordingly, our results showed an increased expression of the GABAergic amacrine cells marker parvalbumin mRNA in the mutant retina (Fig. 6), confirming that loss of *En2* markedly affects the expression profile of GABAergic neurons. Indeed, altered expression of GABAergic markers has been reported in different brain areas following deletion of the *En2* gene (Sudarov and Joyner, 2007; Tripathi et al., 2009; Sgadò et al., 2013; Allegra et al., 2014; Soltani et al., 2017; Boschian et al., 2018). However, since amacrine cell characterization was based on the analysis of a limited number of markers (calbindin and parvalbumin), it remains possible that the overall number of amacrine cells is unchanged in the *En2*$^{-/-}$ retina, while only the gene expression profile of specific subtypes is altered.

Impaired scotopic ERG response in *En2*$^{-/-}$ adult mice

Molecular and structural alteration in photoreceptors and other cell types were accompanied by functional defects in the adult *En2*$^{-/-}$ retina. Specifically, scotopic ERG revealed a significant reduction of both a-wave and b-wave amplitude in *En2*$^{-/-}$ mice, as compared to controls (Fig. 7). To verify the level of visual defect in *En2*$^{-/-}$ mice, we calculated the b-wave/a-wave ratio at maximal flash intensity (Piano et al., 2016) in both genotypes. The values obtained in the two groups of animals were almost superimposable, indicating that the b-wave reduction recorded in *En2*$^{-/-}$ mice is proportional and related to the a-wave reduction. This suggests that the visual defect present in the En2$^{-/-}$ retina primarily resides at the level of rod photoreceptors and is amplified during the passage of the visual signal to bipolar cells. Photopic ERG responses were instead unchanged in *En2*$^{-/-}$ mice (Fig. 8). These results clearly

show that the deletion of the *En2* gene significantly affects rod (scotopic response) but not cone (photopic response) function. These electrophysiological results are in agreement with our expression data, showing a downregulation of rhodopsin mRNA and protein dimer (Fig. 2), as well as *Pcp2* mRNA (Fig. 4) in the mutant retina. Interestingly, a recent study revealed that rhodopsin dimerization is essential for the correct folding, maturation, and targeting of rhodopsin (Zhang et al., 2016), suggesting that physiological function of rhodopsin-mediated phototransduction could be altered in the *En2*$^{-/-}$ retina due to impaired rhodospin dimerization. *Pcp2* is supposed to be expressed only in ON bipolar cells (Xu et al., 2008). Thus, altered *Pcp2* expression actually fits with the functional (ERG) defects observed in mutant mice.

Retinal defects and their relevance for aberrant visual processing in ASD

Several studies show altered sensory processing in ASD patients, including deficits of visual function (reviewed in Lavoie et al., 2014; Robertson and Baron-Cohen, 2017). At the level of the visual cortex, major alterations in visual processing associated to ASD include preference for high contrast, atypical perception of global motion and weaker binocular rivalry, accompanied by lower levels of GABA (Robertson and Baron-Cohen, 2017). As regarding retinal function, a couple of ERG studies have been performed in ASD patients, consistently showing markedly reduced b-wave amplitude in both scotopic (Ritvo et al., 1988; Realmuto et al., 1989) and photopic (Constable et al., 2016) conditions. These results suggest that this particular ERG anomaly may represent a risk biomarker for ASD; in this respect, studies performed on mice lacking ASD-associated genes may be informative. Mice lacking the *Fmr1* gene, a model for Fragile X Syndrome (the most common form of mental retardation with ASD features), display significantly decreased content of

rhodopsin and reduced scotopic ERG b-wave amplitude (Rossignol et al., 2014). This is in agreement with what observed in the *En2*$^{-/-}$ retina, suggesting that in both mutants impaired rhodopsin function might be at the origin of the impaired visual signal transmission between photoreceptors and the inner retina. A recent study showed that retinal molecular defects in *Fmr1* mutant mice are present before eye opening and are maintained throughout adulthood, leading to electrophysiological deficits in the absence of any underlying structural changes (Perche et al., 2018). Interestingly, *Fmr1* expression is down-regulated in the brain of *En2*$^{-/-}$ mice both at mRNA and protein level (Provenzano et al., 2015), and *En2* and *Fmr1* mutant brains share neuroanatomical abnormalities (Ellegood et al., 2015). Taken together, these studies suggest that retinal deficits may impact on visual sensory processing in mice lacking the ASD-associated genes *Fmr1* and *En2*. Indeed, previous studies showed that both *Fmr1* and *En2* mutant mice have impaired visual cortical function (Dölen et al., 2007; Allegra et al., 2014).

Conclusions

In this study, we showed for the first time that anatomical and functional defects are present in the retina of the *En2* ASD mouse model. Our findings are in agreement with similar results obtained in other mouse strains lacking ASD-associated genes. Future work will be needed to understand how the observed retinal defects contribute to altered vision in mouse models of ASD.

ACKNOWLEDGEMENTS

We thank the administrative and technical staff of CIBIO for excellent assistance. The authors declare no conflict of interest. This work was supported by the University of Trento (start-up grant to S.C. and Y.B.). Y.B., S.C. and G.P. are currently supported by the University of Trento 2018-2020 Strategic Project “Trentino Autism Initiative – TRAIN”.

REFERENCES

Ades SE, Sauer RT (1994), Differential DNA-binding specificity of the engrailed homeodomain: the role of residue 50. Biochemistry 33:9187-9194.

Allegra M, Genovesi S, Maggia M, Cenni MC, Zunino G, Sgadò P, Caleo M, Bozzi Y (2014), Altered GABAergic markers, increased binocularity and reduced plasticity in the visual cortex of engrailed-2 kcockout mice. Front Cell Neurosci 8:163. doi: 10.3389/fncel.2014.00163.

Benayed R, Gharani N, Rossman I, Mancuso V, Lazar G, Kamdar S, Bruse SE, Tischfield S, et al. (2005), Support for the homebox transcription factor gene ENGRAILED2 as an autism spectrum disorder susceptibility locus. Am J Hum Genet 77:851-868.

Benayed R, Choi J, Matteson PG, Gharani N, Kamdar S, Brzustowicz LM, Millonig JH (2009), Autism-associated haplotype affects the regulation of the homeobox gene, Engrailed 2. Biol Psychiatry 66:911-917.doi:10.1016/j.biopsych.2009.05.027.

Behrmann M, Thomas C, Humphreys K (2006), Seeing it differently: visual processing in autism. Trends Cogn Sci 10:258-264.

Boschian C, Messina A, Bozza A, Castellini ME, Provenzano G, Bozzi Y, Casarosa S (2018), Impaired neuronal differentiation of neural stem cells lacking the Engrailed-2 gene. Neuroscience 386:137-149.

Brielmaier J, Matteson PG, Silverman JL, Senerth JM, Kelly S, Genestine M, Millonig JH, Dicicco-Bloom E, et al. (2012), Autism-relevant social abnormalities and cognitive deficits in Engrailed-2 knockout mice. PLoS ONE 7:e40914. doi: 10.1371/journal.pone.0040914.

Brunet I, Weinl C, Piper M, Trembleau A, Volovitch M, Harris W, Prochiantz A, Holt C (2005), The transcription factor Engrailed-2 guides retinal axons. Nature 438:94-98.

Chaya T, Matsumoto A, Sugita Y, Watanabe S, Kuwahara R, Tachibana M, Furukawa T (2017), Versatile functional roles of horizontal cells in the retinal circuit. Sci Rep 7:5540. doi: 10.1038/s41598-017-05543-2.

Cheh MA, Millonig JH, Roselli LM, Ming X, Jacobsen E, Kamdar S, Wagner GC (2006), En2 knock out mice display neurobehavioral and neurochemical alterations relevant to autism spectrum disorder. Brain Res, 1116:166-176.

Choi J, Ababon MR, Soliman M, Lin Y, Brzustowicz LM, Matteson PG, Millonig, JH (2014), Autism associated gene, engrailed2, and flanking gene levels are altered in post-mortem cerebellum. PLoS One 9:e87208. doi:10.1371/journal.pone.0087208.

Constable PA, Gaigg SB, Bowler DM, Jägle H, Thompson DA (2016), Full-field electroretinogram in autism spectrum disorder. Doc Ophthalmol 132:83-99.

Dakin S, Frith U (2005), Vagaries of visual perception in autism. Neuron 48:497-507.

Dölen G, Osterweil E, Rao BS, Smith GB, Auerbach BD, Chattarji S, Bear MF (2007), Correction of fragile X syndrome in mice. Neuron 56:955-962.

Ellegood J, Anagnostou E, Babineau BA, Crawley JN, Lin L, Genestine M, DiCicco-Bloom E, Lai JK, Foster JA, Peñagarikano O, Geschwind DH, Pacey LK, Hampson DR, Laliberté CL, Mills AA, Tam E, Osborne LR, Kouser M, Espinosa-Becerra F, Xuan Z, Powell CM, Raznahan A, Robins DM, Nakai N, Nakatani J, Takumi T, van Eede MC, Kerr TM, Muller C, Blakely RD, Veenstra-VanderWeele J, Henkelman RM, Lerch JP (2015), Clustering autism: using neuroanatomical differences in 26 mouse models to gain insight into the heterogeneity. Mol Psychiatry 20:118-125.

Freund CL, Gregory-Evans CY, Furukawa T, Papaioannou M, Looser J, Ploder L, Bellingham J, Ng D, Herbrick JA, Duncan A, Scherer SW, Tsui LC, Loutradis-Anagnostou A, Jacobson SG, Cepko CL,

Bhattacharya SS, McInnes RR (1997), Cone-rod dystrophy due to mutations in a novel photoreceptor-specific homeobox gene (CRX) essential for maintenance of the photoreceptor. Cell 91:543-553.

Furukawa T, Morrow EM, Cepko CL (1997), Crx, a novel otx-like homeobox gene, shows photoreceptor-specific expression and regulates photoreceptor differentiation. Cell 91:531-541.

Gharani N, Benayed R, Mancuso V, Brzustowics LM, Millonig JH (2004), Association of the homebox transcription factor, ENGRAILED2,3, with autism spectrum disorder. Mol Psychiatry 9:474-484.

Gherbassi D, Simon HH (2006), The engrailed transcription factors and the mesencephalic dopaminergic neurons. J Neural Transm Suppl 70:47–55.

Hancock HA, Kraft TW (2004), Oscillatory potential analysis and ERGs of normal and diabetic rats. Invest Ophth Vis Sci 45:1002–1008.

Happé F, Frith U (2006), The weak coherence account: detail-focused cognitive style in autism spectrum disorders. J Autism Dev Disord 36:5-25.

Haverkamp S, Wässle H (2000), Immunocytochemical analysis of the mouse retina. J Comp Neurol 424:1-23.

Haverkamp S, Ghosh KK, Hirano AA, Wässle H (2003), Immunocytochemical description of five bipolar cell types of the mouse retina. J Comp Neurol 455:463-476.

Hnoonual A, Sripo T, Limprasert P (2016), Whole-exome sequencing identifies a novel heterozygous missense variant of the EN2 gene in two unrelated patients with autism spectrum disorder. Psychiatr Genet 26:297-301.

Hughes AE, Enright JM, Myers CA, Shen SQ, Corbo JC (2017) Cell type-specific epigenomic analysis reveals a uniquely closed chromatin architecture in mouse rod photoreceptors. Sci Rep 7:43184. doi: 10.1038/srep43184.

James SJ, Shpyleva S, Melnyk S, Pavliv O, Pogribny IP (2013), Complex epigenetic regulation of engrailed-2 (EN-2) homeobox gene in the autism cerebellum. Transl Psychiatry 3:e232. doi: 10.1038/tp.2013.8.

James SJ, Shpyleva S, Melnyk S, Pavliv O, Pogribny IP (2014), Elevated 5-hydroxymethylcytosine in the Engrailed-2 (EN-2) promoter is associated with increased gene expression and decreased MeCP2 binding in autism cerebellum. Transl Psychiatry 4:e460. doi: 10.1038/tp.2014.87.

Jeon CJ, Strettoi E, Masland RH (1998), The major cell populations of the mouse retina. J Neurosci 18:8936-8946.

Joyner AL (1996), Engrailed, Wnt and Pax genes regulate midbrain—hindbrain development. Trends Genet 12:15-20.

Joyner AL, Herrup K, Auerbach BA, Davis CA, Rossant J (1991), Subtle cerebellar phenotype in mice homozygous for a targeted deletion of the En-2 homebox. Science 251:1239-1343.

Kim JW, Yang HJ, Oel AP, Brooks MJ, Jia L, Plachetzki DC, Li W, Allison WT, Swaroop A (2016), Recruitment of rod photoreceptors from short-wavelength-sensitive cones during the evolution of nocturnal vision in mammals. Dev Cell 37:520-532.

Koulen P, Fletcher EL, Craven SE, Bredt DS, Wässle H (1998), Immunocytochemical localization of the postsynaptic density protein PSD-95 in the mammalian retina. J Neurosci 18:10136-10149.

Kuemerle B, Zanjani H, Joyner A, Herrup K (1997), Pattern deformities and cell Loss in Engrailed-2 mutant mice suggest two separate patterning events during cerebellar development. J Neurosci 17:7881–7889.

Lavoie J, Maziade M, Hébert M (2014), The brain through the retina: the flash electroretinogram as a

tool to investigate psychiatric disorders. Prog Neuropsychopharmacol Biol Psychiatry 48:129-34. doi: 10.1016/j.pnpbp.2013.09.020.

Lei B, Yao G, Zhang K, Hofeldt KJ, Chang B (2006), Study of rod- and cone-driven oscillatory potentials in mice. Invest Ophth Vis Sci 47, 2732–2738.

Mitchell CK, Rowe-Rendleman CL, Ashraf S, Redburn DA (1995), Calbindin immunoreactivity of horizontal cells in the developing rabbit retina. Exp Eye Res 61:691-698.

Mo A, Luo C, Davis FP, Mukamel EA, Henry GL, Nery JR, Urich MA, Picard S, Lister R, Eddy SR, Beer MA, Ecker JR, Nathans J (2016), Epigenomic landscapes of retinal rods and cones. Elife 5:e11613. doi: 10.7554/eLife.11613.

Mottron L, Dawson M, Soulières I, Hubert B, Burack J (2006), Enhanced perceptual functioning in autism: an update, and eight principles of autistic perception. J Autism Dev Disord 36:27-43.

Perche O, Felgerolle C, Ardourel M, Bazinet A, Pâris A, Rossignol R, Meyer-Dilhet G, Mausset-Bonnefont AL, Hébert B, Laurenceau D, Montécot-Dubourg C, Menuet A, Bizot JC, Pichon J, Ranchon-Cole I, Briault S (2018), Early retinal defects in Fmr1(-/y) mice: toward a critical role of visual dys-sensitivity in the fragile X syndrome phenotype? Front Cell Neurosci 12:96. doi: 10.3389/fncel.2018.00096.

Piano I, Novelli E, Della Santina L, Strettoi E, Cervetto L, Gargini C. (2016), Involvement of autophagic pathway in the progression of retinal degeneration in a mouse model of diabetes. Front Cell Neurosci: 10:42. doi: 10.3389/fncel.2016.00042.

Provenzano G, Pangrazzi L, Poli A, Pernigo M, Sgadò P, Genovesi S, Zunino G, Berardi N, et al. (2014a), Hippocampal dysregulation of neurofibromin-dependent pathways is associated with impaired spatial learning in engrailed 2 knock-out mice. J Neurosci 34:13281-13288.

Provenzano G, Sgadò P, Genovesi S, Zunino G, Casarosa S, Bozzi Y. (2015), Hippocampal dysregulation of FMRP/mGluR5 signaling in Engrailed-2 knockout mice, a model of autism spectrum disorders. Neuroreport 26:1101-1105.

Realmuto G, Purple R, Knobloch W, Ritvo E (1989), Electroretinograms (ERGs) in four autistic probands and six first-degree relatives. Can J Psychiatry 34:435-439.

Ritvo ER, Creel D, Realmuto G, Crandall AS, Freeman BJ, Bateman JB, Barr R, Pingree C, Coleman M, Purple R (1988), Electroretinograms in autism: a pilot study of b-wave amplitudes. Am J Psychiatry 145:229-232.

Robertson CE, Baron-Cohen S (2017), Sensory perception in autism. Nat Rev Neurosci 18:671-684.

Rossignol R, Ranchon-Cole I, Pâris A, Herzine A, Perche A, Laurenceau D, Bertrand P, Cercy C, Pichon J, Mortaud S, Briault S, Menuet A, Perche O (2014), Visual sensorial impairments in neurodevelopmental disorders: evidence for a retinal phenotype in Fragile X Syndrome. PLoS One. 9(8):e105996. doi: 10.1371/journal.pone.0105996.

Sgadò P, Genovesi S, Kalinovsky A, Zunino G, Macchi F, Allegra M, Murenu E, Provenzano G, et al. (2013b), Loss of GABAergic neurons in the hippocampus and cerebral cortex of Engrailed-2 null mutant mice: implications for autism spectrum disorders. Exp Neurol 247:496-505.

Siegert S, Cabuy E, Scherf BG, Kohler H, Panda S, Le YZ, Fehling HJ, Gaidatzis D, Stadler MB, Roska B (2012), Transcriptional code and disease map for adult retinal cell types. Nat Neurosci 15:487-495.

Soltani A, Lebrun S, Carpentier G, Zunino G, Chantepie S, Maïza A, Bozzi Y, Desnos C, Darchen F, Stettler O (2017), Increased signaling by the autism-related Engrailed-2 protein enhances dendritic branching and spine density, alters synaptic structural matching, and exaggerates protein synthesis. PLoS One12(8):e0181350. doi: 10.1371/journal.pone.0181350.

Sudarov A, Joyner AL (2007), Cerebellum morphogenesis: the foliation pattern is orchestrated by multi-cellular anchoring centers. Neural Dev 2:26.

Thoreson WB, Mangel SC (2012), Lateral interactions in the outer retina. Prog Retin Eye Res 31:407-441.

Tripathi PP, Sgadò P, Scali M, Viaggi C, Casarosa S, Simon HH, Vaglini F, Corsini GU, et al. (2009), Increased susceptibility to kainic acid-induced seizures in Engrailed-2 knockout mice. Neuroscience 159: 842-849. doi:10.1016/j.neuroscience.2009.01.007.

Vlamings PH, Jonkman LM, van Daalen E, van der Gaag RJ, Kemner C (2010), Basic abnormalities in visual processing affect face processing at an early age in autism spectrum disorder. Biol Psychiatry 68:1107-1113.

Wizenmann A, Brunet I, Lam J, Sonnier L, Beurdeley M, Zarbalis K, Weisenhorn-Vogt D, Weinl C, Dwivedy A, Joliot A, Wurst W, Holt C, Prochiantz A (2009), Extracellular Engrailed participates in the topographic guidance of retinal axons in vivo. Neuron 64:355-366.

Wizenmann A, Stettler O, Moya KL (2015), Engrailed homeoproteins in visual system development. Cell Mol Life Sci 72:1433-1445.

Xu Y, Sulaiman P, Feddersen RM, Liu J, Smith RG, Vardi N (2008), Retinal ON bipolar cells express a new PCP2 splice variant that accelerates the light response. J Neurosci 28:8873-8884.

Zhang T, Cao LH, Kumar S, Enemchukwu NO, Zhang N, Lambert A, Zhao X, Jones A, Wang S, Dennis EM, Fnu A, Ham S, Rainier J, Yau KW, Fu Y (2016), Dimerization of visual pigments in vivo. Proc Natl Acad Sci U S A 113:9093-9098.

FIGURE LEGENDS

Figure 1. ***En2* mRNA is expressed in the adult mouse retina.** A) RT-PCR amplification of *En2* mRNA from *En2*$^{+/+}$ but not *En2*$^{-/-}$ adult mice retina. B) RT-PCR amplification of *En2* mRNA from the outer nuclear layer (ONL), inner nuclear layer (INL), and ganglion cell layer (GCL) collected by laser-capture microdissection of the adult *En2*$^{+/+}$ retina. C), Representative *in situ* hybridization confirming that *En2* mRNA is expressed in the ONL, INL, and GCL of the *En2*$^{+/+}$ but not *En2*$^{-/-}$ adult retina. D) Representative immunostaining showing that En2 protein (red) is expressed in the INL and GCL of the *En2*$^{+/+}$ adult retina. Abbreviations: ONL, outer nuclear layer; INL, inner nuclear layer; GCL, ganglion cells layer. OPL, outer plexiform layer; IPL, inner plexiform layer. Scale bar: 150 μm (C), 100 μm (D).

Figure 2. Rhodopsin expression is reduced in the retina of *En2*$^{-/-}$ adult mice. A) Representative rhodopsin immunohistochemistry (red) on retinal sections from *En2*$^{+/+}$ and *En2*$^{-/-}$ adult mice. Abbreviations: Rho, rhodopsin; ROS, rod outer segment. Scale bar: 25 μm. B) mRNA expression level of rhodopsin, as obtained by qRT-PCR performed on whole retinas of *En2*$^{+/+}$ and *En2*$^{-/-}$ adult mice. Values (box and whiskers plot, median with maximum/minimum) are expressed as rhodopsin/β-actin comparative quantitation ratios (*$p<0.05$, Mann-Whitney U test, *En2*$^{+/+}$ vs. *En2*$^{-/-}$, 3 mice per genotype). C) Rhodopsin immunoblottings from adult mouse retinas of both genotypes; three samples per genotype are shown. Rhodopsin oligomers (Rho olig), dimers (Rho dimer), and monomers (Rho mono) are shown. Glyceraldehyde 3-phosphate dehydrogenase (GAPDH) was used as internal standard; molecular weights (kDa) are indicated on the right. D) Quantification of rhodopsin immunoblotting experiments; rhodopsin dimer levels were normalized to GAPDH (box and whiskers plot, median with maximum/minimum; **$p<0.01$, Mann-Whitney U

test, *En2*$^{+/+}$ vs. *En2*$^{-/-}$, 3 mice per genotype).

Figure 3. Expression of cone photoreceptor markers in the adult retina of *En2*$^{+/+}$ and *En2*$^{-/-}$ adult mice. A) Representative immunostainings showing cone arrestin+ photoreceptors in the retina of *En2*$^{+/+}$ and *En2*$^{-/-}$ adult mice. Abbreviations: OS, outer segment; IS, inner segment; SE, synaptic endings. Scale bar: 25 μm. B) mRNA expression levels of S- and M-opsin, as obtained by qRT-PCR performed on whole retinas of *En2*$^{+/+}$ and *En2*$^{-/-}$ adult mice. Values (box and whiskers plot, median with maximum/minimum) are expressed as each marker/β actin comparative quantitation ratios (3 mice per genotype). C) (Top) S- and M-opsin immunoblottings from adult mouse retinas of both genotypes; three samples per genotype are shown. GAPDH was used as internal standard. (Bottom) Quantification of S- and M-opsin immunoblotting experiments; opsin levels were normalized to GAPDH (box and whiskers plot, median with maximum/minimum; 3 mice per genotype). D) Representative immunostainings showing PSD-95 labelled photoreceptor synaptic terminals (green) in the retina of *En2*$^{+/+}$ and *En2*$^{-/-}$ adult mice. SE, synaptic endings. Scale bar: 50 μm.

Figure 4. Expression of bipolar cell markers in the adult retina of *En2*$^{+/+}$ and *En2*$^{-/-}$ adult mice. A) *Pcp2* mRNA is downregulated in the *En2*$^{-/-}$ retina. mRNA expression was measured by qRT-PCR on whole retinas of *En2*$^{+/+}$ and *En2*$^{-/-}$ adult mice. Values (box and whiskers plot, median with maximum/minimum) are expressed as *Pcp2*/β actin comparative quantitation ratios (***$p<0.001$, Mann-Whitney U test, *En2*$^{+/+}$ vs. *En2*$^{-/-}$, 3 mice per genotype). B) Representative immunostainings showing PKCα-labelled bipolar cells (green) in the retina of *En2*$^{+/+}$ and *En2*$^{-/-}$ adult mice. Scale bar: 25 μm.

Figure 5. Expression of horizontal, amacrine, and ganglion cell markers in the adult retina of *En2*$^{+/+}$ and *En2*$^{-/-}$ adult mice. A, C, E) Representative pictures showing calbindin^{+} horizontal cells (A), calbindin^{+} amacrine/ganglion cells (C), and Brn3a+ ganglion cells (E) in the retina of adult mice from both genotypes. Positive cells are labeled in green. Scale bars: 50µm. B, D, F) Quantification of calbindin and Brn3a cell densities in *En2*$^{+/+}$ and *En2*$^{-/-}$ adult retinas. Values are expressed as labelled cells per mm^2 (box and whiskers plot, median with maximum/minimum; 3-4 mice per genotype; *p<0.05, Mann-Whitney U test, *En2*$^{+/+}$ vs. *En2*$^{-/-}$).

Figure 6. Expression of parvalbumin mRNA in the adult retina of *En2*$^{+/+}$ and *En2*$^{-/-}$ adult mice. Parvalbumin mRNA is upregulated in the *En2*$^{-/-}$ retina. mRNA expression was measured by qRT-PCR on whole retinas of *En2*$^{+/+}$ and *En2*$^{-/-}$ adult mice. Values (box and whiskers plot, median with maximum/minimum) are expressed as parvalbumin/β actin comparative quantitation ratios (**p<0.01, Mann-Whitney U test, *En2*$^{+/+}$ vs. *En2*$^{-/-}$, 3 mice per genotype).

Figure 7. Impairment of scotopic retinal function in *En2*$^{-/-}$ mice. (A) Representative scotopic flash ERG recordings from *En2*$^{+/+}$ and *En2*$^{-/-}$ mice in response to a flash intensity of 377.2 cd*s/m^2, the highest used for all experiments. (B, C) Scotopic a-wave and b-wave amplitude as a function of flash intensity from *En2*$^{+/+}$ and *En2*$^{-/-}$ mice. The traces show impaired ERG function in *En2*$^{-/-}$ mice: both a-wave and b-wave amplitude is significantly reduced. In (B), the graph shows only the luminance values at which the analysis of the 7ms a-wave was carried out (scotopic ERG protocol is normally carried out with a greater number of luminous intensities, see C). (D) Scotopic b-wave peak time (ms) as a function of flash intensity; the kinetics of ERG response is comparable between *En2*$^{+/+}$ and *En2*$^{-/-}$

mice. Note that the flash intensity scale reports only luminance values analyzed at peak time. (E, F) Scotopic OPs amplitude and kinetics, respectively**.** Values are expressed as mean ± s.e.m. (*p<0.05, **p<0.01, Tukey's test following two-way ANOVA, *En2*$^{+/+}$ vs. *En2*$^{-/-}$, 6 mice per genotype).

Figure 8. Preservation of photopic retinal function in *En2*$^{-/-}$ mice. (A) Representative photopic flash ERG recordings from *En2*$^{+/+}$ and *En2*$^{-/-}$ mice in response to a flash intensity of 377 cd*s/m^2 (the highest used for all experiments) superimposed on steady background of 30cd/m^2. (B) Photopic b-wave amplitude as a function of flash intensity from *En2*$^{+/+}$ and *En2*$^{-/-}$ mice. Traces show that cones function is preserved in *En2*$^{-/-}$ mice and the ERG amplitude is the comparable between *En2*$^{+/+}$ and *En2*$^{-/-}$ mice. The graph shows all the luminances used in the photopic ERG protocol, which are the medium and high intensity luminances also used in the scotopic ERG, but are imposed above a fixed background of 30cd/m^2. (C) Photopic b-wave peak time (ms) as a function of flash intensity; the kinetics of ERG response obtained from the cone-pathway is comparable between *En2*$^{+/+}$ and *En2*$^{-/-}$ mice. (D, E) Photopic oscillatory potentials (OP1-OP4) extracted from ERG response to the bright test flash (377cd*s/m^2). Both amplitude and kinetic functions show no difference between *En2*$^{+/+}$ and *En2*$^{-/-}$ mice. Values are expressed as mean ± s.e.m. (p>0.05, two-way ANOVA, *En2*$^{+/+}$ vs. *En2*$^{-/-}$, 6 mice per genotype).

TABLES

Gene name	Forward	Reverse
En1	5′-AGTGGCGGTGGTAGTGGA-3′	5′-CCTTCTCGTTCTTTTTCTTCTTT-3′
En2 (RT-PCR)	5′-ACTGCACGCGCTATTCTG-3′	5′-ACCTGTTGGTCTGAAACTCAG-3′
En2 (ISH)	5′-GCGTAATACGACTCACTATAGGGAAAGGGGACTCTTTAGGGTTTC-3′	5′-CGCATTAACCCTCACTAAAGGGAGAAGATGATTCCAACTCGCTCT-3′
Rhodopsin	5′-GCCTGAGGTCAACAACGAAT-3′	5′-GATAACCATGCGGGTGACTT-3′
M-opsin	5′-CTCTGCTACCTCCAAGTGTGG-3′	5′-AAGGTATAGGGTCCCCAGCAGA-3′
S-opsin	5′-TGTACATGGTCAACAATCGGA-3′	5′-ACACCATCTCCAGAATGCAAG-3′
Pcp2	5′-AGGCTTCTTCAACCTGCAGA-3′	5′-CGTTTCTGCATTCCATCCTT-3′
Parvalbumin	5′-TGCTCATCCAAGTTGCAGG-3‘	5′-GCCACTTTTGTCTTTGTCCAG-3′
β-actin	5′-AATCGTGCGTGACATCAAAG-3′	5′-AAGGAAGGCTGGAAAAGAGC-3′

Table 1. Primers used for RT-PCR and *in situ* hybridization (ISH) experiments.

Antibodies	Use	Dilution	Producer/cat. #
Goat polyclonal anti-EN2	IHC	1:250	Abcam ab45867
Mouse monoclonal anti-rhodopsin	IHC, IB	1:5000	Sigma O4886
Mouse monoclonal anti-GAPDH	IB	1:5000	Santa Cruz sc-32233
Rabbit polyclonal anti-cone arrestin	IHC	1:2000	Millipore AB15282
Rabbit polyclonal anti S-opsin	IB	1:200	Millipore AB5407
Rabbit polyclonal anti M-opsin	IB	1:200	Millipore AB 5405
Mouse monoclonal anti PKC-α	IHC	1:200	Santa Cruz sc-8393
Rabbit monoclonal anti-PSD-95	IHC	1:200	Cell Signaling 3450S
Rabbit polyclonal anti-calbindin D-28k	IHC	1:5000	Swant CB38
Mouse monoclonal anti-Brn3a	IHC	1:500	Millipore MAB1585
Donkey anti-mouse Alexa 488	IHC	1:1000	Life Technologies A-21202
Goat anti-rabbit Alexa 488	IHC	1:1000	Life Technologies A11034
Goat anti-rabbit Alexa 594	IHC	1:1000	Life Technologies A11037
Bovine anti-goat Alexa 594	IHC	1:1000	Jackson ImmunoLab 805-585-1800

Table 2. Antibodies used for immunohistochemistry (IHC) and immunoblotting (IB) experiments.

Marker	Experiment	Direction of change ($En2^{-/-}$ vs. $En2^{+/+}$)
Rhodopsin mRNA	qRT-PCR	decreased
Rhodopsin protein dimer	IB	decreased
cone arrestin	IHC	no change
S opsin mRNA	qRT-PCR	no change
S opsin protein	IB	no change
M opsin mRNA	qRT-PCR	no change
M opsin protein	IB	no change
PSD-95	IHC	no change
Pcp2 mRNA	qRT-PCR	decreased
PKCα	IHC	no change
calbindin^{+} horizontal cells	IHC	decreased
calbindin^{+} amacrine/ganglion cells	IHC	no change
Brn3a^{+} ganglion cells	IHC	no change
parvalbumin mRNA	qRT-PCR	increased

Table 3. Summary of marker expression in *En2*$^{-/-}$ *vs. En2*$^{+/+}$ adult retinas. Abbreviations: IB, immunoblotting, IHC, immunohistochemistry; other abbreviations as in the text.

Retinal defects in mice lacking the autism-associated gene *Engrailed-2*

Xuwen Zhang[1], Ilaria Piano[2], Andrea Messina[3], Vanessa D'Antongiovanni[4], Fabiana Crò[1]*, Giovanni Provenzano[1], Yuri Bozzi[3,5], Claudia Gargini[2], Simona Casarosa[1,5]

[1] Centre for Integrative Biology, University of Trento, Trento, Italy

[2] Department of Pharmacy, University of Pisa, Pisa, Italy

[3] Center for Mind/Brain Sciences (CIMeC), University of Trento, Rovereto, Italy

[4] Department of Clinical and Experimental Medicine, University of Pisa, Italy.

[5] CNR Neuroscience Institute, Pisa, Italy

*present address: Gruppo SYNLAB Italia, Castenedolo, Lombardia, Italia

Correspondence should be addressed to:

Prof. Simona Casarosa,
Laboratory of Neural Development and Regeneration
Centre for Integrative Biology (CIBIO)
Via Sommarive 9, 38123 Trento, Italy
email: simona.casarosa@unitn.it

Prof. Yuri Bozzi,
Neurodevelopmental Disorders Research Group
Center for Mind/Brain Sciences (CIMeC), University of Trentoi
Corso Bettini 31, Rovereto (TN), Italy
email: yuri.bozzi@unitn.it

Abstract

Defective cortical processing of visual stimuli and altered retinal function have been described in autism spectrum disorder (ASD) patients. In keeping with these findings, anatomical and functional defects have been found in the visual cortex and retina of mice bearing mutations for ASD-associated genes. Here we sought to investigate the anatomy and function of the adult retina of *Engrailed 2* knockout *(En2$^{-/-}$)* mice, a model for ASD. Our results showed that *En2* is expressed in all three nuclear layers of the adult retina. When compared to age-matched *En2$^{+/+}$* controls, *En2$^{-/-}$* adult retinas showed a significant decrease in the number of calbindin^{+} horizontal cells, and a significant increase in calbindin^{+} amacrine/ganglion cells. The total number of ganglion cells was not altered in the adult *En2$^{-/-}$* retina, as shown by *Brn3a^{+}* cell counts. In addition, *En2$^{-/-}$* adult mice showed a significant reduction of photoreceptor (rhodopsin) and bipolar cell (*Pcp2,* PKCα) markers. Functional defects were also present in the retina of *En2* mutants, as indicated by electroretinogram recordings showing a significant reduction in both a-wave and b-wave amplitude in *En2$^{-/-}$* mice as compared to controls. These data show for the first time that anatomical and functional defects are present in the retina of the *En2* ASD mouse model.

KEYWORDS

Retina, electroretinogram, neurodevelopmental disorder, vision, photoreceptor.

ABBREVIATIONS

ASD, autism spectrum disorders

BSA, bovine serum albumin

En2, Engrailed-2

ERG, electroretinogram

GABA, γ-aminobutyric acid

GAPDH, glyceraldehyde 3-phosphate dehydrogenase

GCL, ganglion cell layer

IB, immunoblotting

IHC, immunohistochemistry

INL, inner nuclear layer

ONL, outer nuclear layer

OP, oscillatory potential

OS, outer segment

PFA, paraformaldehyde

PKCα, protein kinase Cα

PSD-95, postsynaptic density protein 95

qRT-PCR, quantitative reverse transcription PCR

Rho, rhodopsin

ROS, rod outer segment

SDS-PAGE, sodium-dodecyl-sulphate polyacrylamide gel electrophoresis

VEP, visual evoked potentials

Introduction

The *Engrailed-2* (*En2*) gene is a homeobox-containing transcription factor, involved in the regionalization, patterning and neural differentiation of the midbrain/hindbrain region (Joyner et al., 1991; Joyner, 1996). *En2* is widely expressed in the midbrain/hindbrain region (including the cerebellum primordium), starting at embryonic day 8.5 and continuing throughout embryonic and postnatal development (Joyner 1996; Gherbassi and Simon, 2006). *En2* mRNA is also expressed in the hippocampus and cerebral cortex of adult mouse (Tripathi et al., 2009; Sgadò et al., 2013). Mice lacking the homeobox-containing transcription factor *En2* (*En2*$^{-/-}$) are a reliable model for investigating the neurodevelopmental basis of autism spectrum disorders (ASD). Genetic studies (Gharani et al., 2004; Benayed et al., 2005, 2009; Hnoonual et al., 2016) and expression analyses on post-mortem brain tissues (James et al., 2013, 2014; Choi et al., 2014) showed that deregulated expression of the human EN2 gene is linked to ASD.

En2$^{-/-}$ mice display ASD-like behaviors (Cheh et al., 2006; Brielmaier et al., 2012; Provenzano et al., 2014) accompanied by ASD-relevant anatomical deficits, including cerebellar hypoplasia (Joyner et al., 1991; Kuemerle et al., 1997) and loss of GABAergic interneurons in somatosensory (Sgadò et al., 2013) and visual cortical (Allegra et al., 2014) areas. Interneuron defects in the *En2*$^{-/-}$ visual cortex are accompanied by altered binocularity and reduced visual cortical plasticity, while visual functional properties (acuity, response latency, receptive field size) are unaffected in *En2*$^{-/-}$ mutant mice (Allegra et al., 2014).

Sensory processing has been given an increasing attention in both ASD diagnosis and research in recent years (Robertson and Baron-Cohen, 2017). Enhanced visual evoked potentials (VEP) responses to high spatial frequencies were found in visual brain areas of ASD children, while unaffected control children

generally responded to visual stimuli with low spatial frequency (Vlamings et al., 2010). This is in agreement with previous studies showing that visual perception in ASD is more detail-oriented, suggesting that primary visual processing might also contribute to social and communication deficits in ASD (Dakin and Frith, 2005; Happé and Frith, 2006; Mottron et al., 2006; Behrmann et al., 2006). In addition, defective retinal function has been described in human ASD patients (Lavoie et al., 2014; Constable et al., 2016).

In keeping with these findings, anatomical and functional defects were found in the retina of *Fmr1* knockout mice (Rossignol et al., 2014), a syndromic ASD model sharing neuroanatomical (Ellegood et al., 2015) and molecular (Provenzano et al., 2015) abnormalities with *En2*$^{-/-}$ mice. To understand whether retinal defects are a common neuropathological feature in ASD mouse models, here we sought to investigate the morphology and function of the *En2*$^{-/-}$ adult retina.

EXPERIMENTAL PROCEDURES

Animals. All experimental procedures were performed in accordance with the European Communities Council Directive 2010/63/EU and were approved by the Animal Welfare Committee of the University of Trento and the Italian Ministry of Health. Animals were housed in a 12h light/dark cycle with food and water available *ad libitum,* and all efforts were made to minimize animals' suffering during experimental procedures. The original *En2* mutant strain (mixed 129Sv × C57BL/6 genetic background; Joyner et al., 1991) was backcrossed at least five times into a C57BL/6 background (Sgadò et al., 2013). Heterozygous matings ($En2^{+/-}$ × $En2^{+/-}$) were used to obtain $En2^{+/+}$ and $En2^{-/-}$ littermates used in this study. Mice were genotyped according to published protocols (www.jax.org; mouse strain $En2^{tm1Alj}$). All experiments were performed on adult animals (3-5 months old; weight = 25-35 g) of both sexes, since previous studies showed that behavioral traits and gene expression profiles did not differ between genders in both $En2^{+/+}$ and $En2^{-/-}$ mice (Brielmaier et al., 2012; Sgadò et al., 2013). A total of 66 mice were used in this study. Twelve mice (6 per genotype) were used for quantitative reverse transcription PCR (qRT-PCR) and laser-capture microdissection, 6 (3 per genotype) for *in situ* hybridization, 8 (4 per genotype) for immunohistochemistry on retinal sections, 22 (11 per genotype) for whole-mount immunohistochemistry, 6 (3 per genotype) immunoblotting, and 12 (6 per genotype) for electroretinogram (ERG). For anatomy and gene expression experiments, eyes were rapidly removed after cervical dislocation. For ERG, mice received 20% urethane (0.1ml/10g of body weight) and were sacrificed at the end of the experiment by cervical dislocation without awakening from anesthesia.

Laser-capture microdissection. Eyes from adult *En2*$^{+/+}$ mice were embedded in Tissue-Tek O.C.T. compound (Sakura-VWR), frozen on dry ice, and stored at -80°C. Frozen tissues were cut into 12 µm thick sections and collected on RNase-free polyethylene naphthalate membrane slides (Leica). Sections were then thawed and fixed in 75% ethanol for 30s, counterstained with hematoxylin and eosin for 45 s, and washed in RNase-free water for 30 s. Finally, the sections were dehydrated in graded ethanol and air-dried. Three retinal layers (ganglion cell layer, inner nuclear layer, and outer nuclear layer) were dissected on a laser capture microdissection (LCM) system (LMD6500, Leica). Total RNA was extracted from the captured layers by using the PicoPure RNA Isolation Kit (Life Technologies). On-column digestion with RNase-Free DNase Set (Qiagen) was performed to ensure the removal of possible genomic DNA contamination. Samples were reversed transcribed and subjected to qRT-PCR analysis.

In situ hybridization. Eyes from *En2*$^{+/+}$ and *En2*$^{-/-}$ mice were rapidly removed and fixed by immersion in 4% PFA after removal of the cornea and lens. After fixation, the eyecups were cryoprotected in 20% sucrose, embedded in Tissue-Tek O.C.T. compound (Sakura-VWR), and 12 µm thick cryostat sections were serially cut (Leica CM1850). Non-radioactive *in situ* hybridization was performed as previously described (Tripathi et al., 2009) using a digoxigenin-labeled *En2* riboprobe (Genbank ID: NM_010134). The *En2* antisense riboprobe was generated from a T3 RNA polymerase promoter flanking a cDNA fragment of approximately 440 base pairs generated by RT-PCR from cerebellar RNA. Primers used for *in situ* hybridization are listed in Table 1. Signal was detected by alkaline phosphatase–conjugated anti-digoxigenin antibody followed by alkaline phosphatase staining. Stained sections

were photographed using an AxioCam MRm camera connected to a Zeiss Axio Imager M2 microscope (Carl Zeiss).

qRT-PCR. Total RNAs from *En2*$^{+/+}$ and *En2*$^{-/-}$ mice eyes were extracted by Nucleospin RNA XS kit (Macherey-Nagel). cDNA was synthesized from the total RNAs (1µg) by SuperScript VILO cDNA Synthesis Kit (Invitrogen). qRT-PCR was performed in a C1000 Thermal Cycler (Bio-Rad) with real-time detection of fluorescence, using the KAPA SYBR FAST Master Mix reagent (KAPA Biosystems). Mouse beta-actin (β-actin) was used as an internal standard for quantification analysis. Primers used for qRT-PCR are reported in Table 1. Ratios of comparative concentrations of each mRNA with respect to β-actin mRNA were then calculated and plotted as the average of three independent reactions with technical replicates obtained from each RNA sample. Expression analysis was performed using the CFX3 Manager (BioRad) software.

Immunohistochemistry. Eyes from *En2*$^{+/+}$ and *En2*$^{-/-}$ mice were rapidly removed and fixed by immersion in 4% paraformaldehyde (PFA) after removal of the cornea and lens. For immunohistochemistry on whole-mounted retinas, retinas were crosscut in 1x PBS to flatten them. For immunohistochemistry on sections, eyecups were cryoprotected in 20% sucrose, embedded in Tissue-Tek O.C.T. compound (Sakura-VWR), and serially cut (12 µm thick) at the cryostat (Leica CM1850).

Immunohistochemistry was performed as follows: whole-mounted retinas were incubated in blocking solution containing 0.3% Triton X-100 and 5% BSA in 1x PBS overnight at 4°C followed by 3 days of incubation in 0.1% Triton X-100 and 1% BSA in 1×PBS at 4°C in a stable agitator, with the primary antibody. Cryostat sections

were blocked in blocking solution containing 0.5% Triton X-100, 1% BSA and 10% fetal bovine serum in 1x PBS at room temperature for 1hr followed by overnight incubation at 4°C with 0.5% Triton X-100, 1% BSA, and 3% FBS in 1x PBS, with primary antibodies. Samples were then incubated 2 days (flat-mounts at 4°C) or 2hrs (sections at room temperature) with secondary antibodies conjugated to either Alexa 488 or Alexa 594, washed in 1x PBS and mounted onto glass slides using Aqua-Poly/Mount coverslipping medium (Polysciences, Inc.). Primary and secondary antibodies used are listed in Table 2.

***Image acquisition and cell counting*.** Image stacks were acquired using a Zeiss Axio Observer Z1 microscope (Zeiss) equipped with Axiocam 503 mono camera. Full mosaic images of whole mount retina tissues were acquired by the tile function of the microscope using an EC Plan-Neofluar 20x or 40x objective for the quantitative analysis of calbindin$^+$ horizontal/amacrine/ganglion cells or Brn-3a$^+$ ganglion cells. Z-plane, exposure time and microscope settings were optimized for each marker and cell type, and then kept constant in all acqisitions for both genotypes. For cell counting, 8 tile images in the central part of each wing of the retina were extracted, therefore a total of 32 tile images were extracted per retina per genotype to count cells. Cell counting was performed by Columbus software (PerkinElmer) or Image J software (NIH) in a consistent way. Parameters (common threshold, area, split factor, individual threshold, contrast, cell roundness) for defining and selecting the objective cells were optimized for each marker using the Columbus software. All the images for each specific marker, from both genotypes, were analyzed under the same set of parameters in the Columbus software. Cell counting for calbindin$^+$ amacrine/ganglion cells was performed manually by using Image J. Cell densities were then plotted as the total number of positive cells in total counting area.

Immunoblotting. Total proteins were extracted from *En2*$^{+/+}$ and *En2*$^{-/-}$ eyes using a standard protocol, under reducing conditions. Total protein extracts were separated by standard SDS-PAGE, blotted and incubated with the different antibodies, as indicated in Table 2. Immunoblots were revealed and quantified using chemiluminescence followed by densitometry using Image J (NIH). GAPDH was used as an internal standard for protein quantification analysis.

Electroretinogram (ERG) recordings. ERGs were recorded from dark-adapted mice by means of coiled gold electrodes making contact with the cornea moisturized by a thin layer of gel. Pupils were fully dilated by application of a drop of 1% atropine (Farmigea, Pisa, Italy). Scotopic ERG recordings were average responses (n = 5) to flashes of increasing intensity (1.7×10^{-5} to 377.2 cd*s/m^2, 0.6 log units steps) presented with an inter-stimulus interval ranging from 20 s for dim flashes to 1 min for the brightest flashes. Isolated cone (photopic) components were obtained by superimposing the test flashes (0.016 to 377.2 cd*s/m^2, 0.6 log units steps) on a steady background of saturating intensity for rods (30 cd/m^2), after at least 15 min from background onset. Amplitude of the a-wave was measured at 7 ms after the onset of light stimulus and the b-wave was measured from the peak of the a-wave to the peak of the b-wave. Oscillatory potentials (OPs) were also measured in both scotopic and photopic conditions. OPs were extracted digitally by using a fifth-order Butterworth filter as previously described (Hancock et al., 2004; Lei et al., 2006). Peak amplitude of each OP (OP1–OP4) was measured. ERG data for each condition of light-induction were collected from 6 animals per genotype.

Statistical analyses. Statistical analysis was performed by Prism 6 software (GraphPad). qRT-PCR, immunoblotting and immunohistochemistry data were analysed with a non-parametric (Mann-Whitney U) test (*En2*$^{+/+}$ vs. *En2*$^{-/-}$). ERG data were analysed by two-way ANOVA (factors: genotype and flash intensity) followed by post-hoc Tuckey test for multiple comparisons. Values of b-wave/a-wave ratio of scotopic ERG were analysed by Student's t-test. In all tests, statistical significance level was set at $p<0.05$.

RESULTS

***En2 is expressed in adult mouse retina*.** We first investigated whether *En2* is expressed in the adult mouse retina. To this aim, we performed RT-PCR on RNAs extracted from whole retinas and from the three retinal nuclear layers obtained by laser-capture microdissection. RT-PCR showed that *En2* mRNA was expressed in the retina of $En2^{+/+}$ but not $En2^{-/-}$ adult mice (Fig. 1A). *Engrailed 1* (*En1*) mRNA, whose expression largely overlaps with that of *En2* (Joyner, 1996), was not detected in the retina of $En2^{+/+}$ nor $En2^{-/-}$ adult mice (data not shown). *En2* mRNA was localized in all three nuclear layers (Fig. 1B), as confirmed by *in situ* hybridization (Fig. 1C). Immunohistochemistry with an En2-specific antibody revealed that En2 nuclear staining was localized in the inner nuclear (INL) and ganglion cell (GCL) layers, but not in the photoreceptor cell (outer nuclear, ONL) layer (Figure 1D).

Rhodopsin expression is downregulated in the $En2^{-/-}$ adult retina. Since *En2* is expressed in all three nuclear layers of the adult mice retina, we asked whether retinal neurons are affected in the absence of *En2*. We first characterized rod photoreceptors, which account for the majority of photoreceptors in the mouse retina [Jeon et al., 1998; Haverkamp and Wässle, 2000]. We first performed immunohistochemistry on $En2^{+/+}$ and $En2^{-/-}$ retinal sections using the rod photoreceptor specific marker rhodopsin, which labels the rod outer segment (ROS) disk membrane. Rhodopsin immunohistochemistry did not show significant differences between $En2^{-/-}$ and $En2^{+/+}$ ROS (Fig. 2A). qRT-PCR analysis showed a significant downregulation of rhodopsin mRNA in the $En2^{-/-}$ retina ($p<0.05$, Mann-Whitney U test, $En2^{+/+}$ vs. $En2^{-/-}$; n=3 per genotype; Fig. 2B). In keeping with these findings, immunoblotting experiments showed that the rhodopsin dimer isoform (78 kDa) was significantly downregulated in the $En2^{-/-}$ mice retina, as compared to $En2^{+/+}$

controls ($p<0.01$, Mann-Whitney U test, *En2*$^{+/+}$ vs. *En2*$^{-/-}$; n=3 per genotype; Fig. 2C). Levels of rhodopsin oligomer (114 kDa, Fig. 2C) and monomer (40 kDa, not shown) isoforms did not differ between genotypes.

Cone photoreceptor markers are unchanged in the En2$^{-/-}$ adult retina. We next investigated the expression of cone photoreceptor markers in *En2*$^{+/+}$ and *En2*$^{-/-}$ adult retinas. Immunohistochemistry for the cone photoreceptor marker cone-arrestin showed that the structure of the outer segment (OS) of cone photoreceptors is comparable between *En2*$^{-/-}$ and *En2*$^{+/+}$ mice (Fig. 3A). In the mouse retina, there are two subtypes of cone photoreceptors: short-wavelength (blue) sensitive cones (S-cones) and medium-wavelength (green/red) sensitive cones (M-cones), which express different types of opsins (S opsin and M opsin, respectively). qRT-PCR showed comparable levels of S opsin and M opsin mRNAs in adult *En2*$^{+/+}$ and *En2*$^{-/-}$ retinas ($p>0.05$, Mann-Whitney U test, *En2*$^{+/+}$ vs. *En2*$^{-/-}$, 3 mice per genotype; Fig. 3B). Similarly, immunoblotting experiments did not reveal any significant changes of S and M opsin protein levels between the two genotypes ($p>0.05$, Mann-Whitney U test, *En2*$^{+/+}$ vs. *En2*$^{-/-}$; n=3 per genotype; Fig. 3C). Finally, to understand whether photoreceptor synaptic terminals were altered in the *En2*$^{-/-}$ mice retina, we performed immunohistochemistry for postsynaptic density protein 95 (PSD- 95), which strongly labels the excitatory axon terminals of rods and cones in the outer plexiform layer (Koulen et al., 1998). PSD-95 labelled photoreceptor synaptic terminals showed no difference between *En2*$^{+/+}$ and *En2*$^{-/-}$ mice (Fig. 3D).

Altered expression of bipolar cell markers in the En2$^{-/-}$ adult retina. Photoreceptor cells transmit their signals to bipolar cells. To characterize bipolar cells, we first performed qRT-PCR for the specific marker Purkinje cell protein 2

(*Pcp2*; Xu et al., 2008). *Pcp2* mRNA showed a significant reduction in the *En2*$^{-/-}$ adult retina, as compared to age-matched *En2*$^{+/+}$ controls ($p<0.001$, Mann-Whitney U test, *En2*$^{+/+}$ vs. *En2*$^{-/-}$, 3 mice per genotype; Fig. 4A). Immunohistochemistry for the bipolar cells marker protein kinase Cα (PKCα Haverkamp et al., 2003) did not reveal significant differences between *En2*$^{-/-}$ and *En2*$^{+/+}$ adult retinas (Fig. 4B).

Decreased density of calbindin^{+} horizontal cells in the En2$^{-/-}$ adult mouse retina. In the mouse retina, horizontal cells laterally interconnect with photoreceptors and bipolar cells. To characterize these cells, we performed whole-mount immunohistochemistry experiments on *En2*$^{+/+}$ vs. *En2*$^{-/-}$ retinas using the specific marker calbindin (Mitchell et al., 1995). Calbindin^{+} horizontal cell density was significantly reduced in the *En2*$^{-/-}$ adult retina, as compared to *En2*$^{+/+}$ controls (Fig. 5A). Quantification of cell counts confirmed these findings ($p<0.05$, Mann-Whitney U test, n=4 mice per genotype; Fig. 5B).

Increased density of calbindin^{+} amacrine and ganglion cells in the En2$^{-/-}$ adult mouse retina. In the mouse retina, calbindin is known to stain also amacrine cells in the inner part of the INL, ganglion cells, and displaced amacrine cells in the GCL. We therefore selectively acquired calbindin immunofluorescence in the INL/GCL of *En2*$^{+/+}$ and *En2*$^{-/-}$ mice whole retinas (Fig. 5B). Quantification of cell counts showed a statistically significant increase of calbindin^{+} amacrine/ganglion cell density in *En2*$^{-/-}$ retina, as compared to aged-matched *En2*$^{+/+}$ controls ($p<0.05$, Mann-Whitney U, n=4 mice per genotype; Fig. 5D). In keeping with these findings, qRT-PCR experiments showed significantly increased mRNA levels of the GABAergic amacrine marker parvalbumin in the *En2*$^{-/-}$ retina, as compared to *En2*$^{+/+}$ controls ($p<0.01$, Mann-Whitney U test, *En2*$^{+/+}$ vs. *En2*$^{-/-}$, 3 mice per genotype; Fig. 6). We finally investigated

retinal ganglion cell density by brain-specific homeobox/POU domain protein 3a (Brn3a) immunohistochemistry on *En2*$^{+/+}$ and *En2*$^{-/-}$ whole-mounted retinas (Fig. 5E), which revealed no significant difference between the two genotypes ($p>0.05$, Mann-Whitney U test, *En2*$^{+/+}$ vs. *En2*$^{-/-}$, 3 mice per genotype; Fig. 5F).

Impairment of scotopic retinal function in En2*$^{-/-}$ *mice. Retinal function was evaluated by both scotopic and photopic ERG recordings. *En2*$^{-/-}$ mice showed a reduction in scotopic ERG response, as compared to *En2*$^{+/+}$ age-matched controls (Fig. 7A). The amplitude of the 7ms a-wave, which represents the inhibition of rod dark-current, showed a significant reduction in *En2*$^{-/-}$ animals as compared to *En2*$^{+/+}$ (two-way ANOVA; main effect of genotype $F_{(1,84)}=6.796$, $p = 0.012$; main effect of flash intensity $F_{(1,84)}=15.748$, $p<0.001$; Tukey's test following two-way ANOVA; *En2*$^{+/+}$ vs. *En2*$^{-/-}$ at 377.2 cd*s/m^2, $p<0.01$; n=6 per genotype; Fig. 7B). The b-wave amplitude was also significantly reduced in *En2*$^{-/-}$ mice, as compared to *En2*$^{+/+}$ controls (two-way ANOVA; main effect of genotype $F_{(1,144)}=41.187$, $p<0.001$; main effect of flash intensity $F_{(1,144)}=25.434$, $p=0$; Tukey's test following two-way ANOVA, *En2*$^{+/+}$ vs. *En2*$^{-/-}$ $p<0.01$ at 377.2 and 83.7 cd*s/m^2, $p<0.05$ at flash intensity level between 1.29 and 21.2 cd*s/m^2; n=6 per genotype; Fig. 7C). In order to investigate where the functional changes originate, we analyzed the b-wave/a-wave ratio of scotopic ERG (Piano et al., 2016). This ratio, measured at maximal flash intensity (377.2 cd*s/m^2), was comparable in *En2*$^{+/+}$ and *En2*$^{-/-}$ mice (*En2*$^{+/+}$, 7.71±1.58; *En2*$^{-/-}$, 8.51±1.0; $p>0.05$, Student's *t*-test, *En2*$^{+/+}$ vs. *En2*$^{-/-}$; n=6 per genotype). This suggests that the reduction of b-wave amplitude observed in *En2*$^{-/-}$ mice directly depends on the reduction of the a-wave amplitude, indicating a defect in rod photoreceptors in mutant mice. Conversely, the kinetics of the response (Fig. 7D) and scotopic OPs amplitude (Fig. 7E) did not differ between *En2*$^{-/-}$ and *En2*$^{+/+}$ mice. No difference

between the two genotypes was found when evaluating the scotopic peak time (kinetic response; Fig. 7F).

Preservation of photopic retinal function in En2$^{-/-}$ mice. Figure 8 shows the results obtained from the photopic ERG recordings. The amplitude of the photopic b-wave showed no difference between *En2*$^{-/-}$ and *En2*$^{+/+}$ mice, and also the kinetics was completely superimposable between the two genotypes. The analysis of OPs also showed no difference between *En2*$^{-/-}$ and *En2*$^{+/+}$ mice.

DISCUSSION

Brief summary of results

In this study, we showed that the ASD-associated gene *En2* is expressed in all three nuclear layers of the adult retina. Immunohistochemical analyses showed a significantly reduced expression of photoreceptor and bipolar cell markers in *En2*$^{-/-}$ retinas, accompanied by a significantly altered number of calbindin^{+} horizontal and amacrine/ganglion cells (Table 3). ERG recordings showed a significant reduction in scotopic a-wave and b-wave amplitude in *En2*$^{-/-}$ mice, as compared to controls. These data show for the first time that anatomical and functional defects are present in the retina of the *En2* mutant mice.

En2 is expressed in the adult mouse retina

Previous studies showed from our and other laboratories clearly showed that *En2* mRNA, in addition to being expressed in the developing mesencephalon and cerebellum, is also detected in several areas of the postnatal forebrain, including the hippocampus and neocortex (Tripathi et al., 2009; Brielmaier J., 2012; Sgadò et al, 2013; Allegra et al., 2014; Provenzano et al., 2014; Soltani et al., 2018). The present study confirms that *En2* is expressed in anterior regions of the central nervous system. Our data show that *En2* mRNA is present in all nuclear layers of the adult mouse retina, while En2 protein nuclear staining is detected in INL and GCL but not in the photoreceptor layer. A previous study reported a selective *En2* mRNA expression in cone photoreceptors (Siegert et al., 2012), and more recent RNA sequencing datasets showed minimal or no expression of *En2* in purified rod photoreceptors (Kim et al., 2016; Mo et al., 2016; Hughes et al., 2017). Our non-quantitative RT-PCR data from laser-capture microdissected retinal layers do not allow us to identify the cell types expressing En2 mRNA. Moreover, it should also be

considered that *En2* mRNA signal could result from Müller glia cells, whose cell bodies are present in all three retinal cell layers. Thus, our *in situ* hybridization data showing *En2* mRNA expression in the photoreceptor layer should be interpreted with extreme caution. Expression of En2 in the INL/GCL was instead corroborated by immunostaining, suggesting that the En2 protein is present in amacrine and possibly ganglion cells (Fig. 1D).

_En2_ inactivation alters rod photoreceptor and bipolar cell marker expression

The expression profile of *En2* in the adult retina led us to investigate whether *En2* gene inactivation resulted in retinal structural and/or functional defects. We first observed a significant down-regulation of the rod photoreceptor-specific marker rhodopsin the *En2*$^{-/-}$ retina, at both mRNA and protein level (Fig. 2). Cone photoreceptor markers were instead unchanged in the *En2*$^{-/-}$ retina (Fig. 3). The reduction of rhodopsin might be caused by the loss of *En2* transcriptional regulation, as a similar effect was observed in the absence of other homeobox transcription factors. As an example, mice lacking *Crx,* a photoreceptor-specific transcription factor, show a disrupted morphogenesis of the photoreceptor outer segment, and fail to produce the phototransduction apparatus (Furukawa et al., 1997). En2, as Crx, binds the DNA sequence TAATTC/A (Ades and Sauer, 1994), which is found upstream of several photoreceptor-specific genes (Freund et al., 1997), and this might explain the altered expression of photoreceptor markers observed in *En2*$^{-/-}$ mice. However, it remains to be investigated how the loss of En2, which is virtually absent from rod photoreceptors (Kim et al., 2016; Mo et al., 2016; Hughes et al., 2017; and see also Fig. 1D), might result in rod phototransduction defects. Previous work showed that a gradient of Engrailed proteins secreted by tectal neurons is able to guide retinal axon growth in a topographical manner (Brunet et al., 2005;

Wizenmann et al., 2009). Although secretion of Engrailed proteins by retinal cells has not been shown so far (Wizenmann et al., 2015), in principle we can not exclude that En2 expressed in the INL (Figure 1) and secreted by INL neurons can act on other retinal cell types.

Bipolar cell markers were also affected in the *En2*$^{-/-}$ retina. Our results showed a significant reduction of the mRNA for the bipolar cell marker *Pcp2*, as compared to age-matched controls; *En2*$^{-/-}$ bipolar cells also showed shorter axons, as revealed by PKCα immunohistochemistry (Fig. 4). This suggests the absence of the *En2* transcription factor also impacts on the transcriptomic profile of rod bipolar cells, which express *Pcp2* (Xu et al., 2008) and PKCα (Haverkamp et al., 2003). It is however important to point out that in this study we did not count the number of photoreceptors and bipolar cells. Therefore, it remains unclear whether the observed physiological defects arise from changes in gene expression of the investigated markers, or in the numbers of these cell subtypes.

Altered cells density of horizontal and amacrine cells in the *En2*$^{-/-}$ retina

Horizontal cells modulate the lateral signal transmission neurotransmission between the photoreceptors and bipolar cells. Negative feedback from horizontal cells to cones and direct feed-forward input from horizontal cells to bipolar cells are responsible for generating center-surround receptive fields that enhance spatial discrimination (Thoreson and Mangel, 2012). Our results a significant reduction of calbindin^{+} horizontal cells in the *En2*$^{-/-}$ retina (Fig. 5A, B). Mice lacking horizontal cells show multiple functional defects, such as altered firing properties and receptive field formation of retinal ganglion cells, impaired ambient light adaptation, and altered optokinetic responses (i.e., reflexive eye movements elicited by a moving visual pattern) (Chaya et al., 2017). Thus, partial loss of horizontal cells in the *En2*$^{-/-}$ retina

might affect several different aspects of visual processing; further studies are needed to elucidate the impact of reduced horizontal cell density in *En2*$^{-/-}$ mice.

Amacrine cell density was instead increased in the *En2*$^{-/-}$ retina (Fig. 5C, D); accordingly, our results showed an increased expression of the GABAergic amacrine cells marker parvalbumin mRNA in the mutant retina (Fig. 6), confirming that loss of *En2* markedly affects the expression profile of GABAergic neurons. Indeed, altered expression of GABAergic markers has been reported in different brain areas following deletion of the *En2* gene (Sudarov and Joyner, 2007; Tripathi et al., 2009; Sgadò et al., 2013; Allegra et al., 2014; Soltani et al., 2017; Boschian et al., 2018). However, since amacrine cell characterization was based on the analysis of a limited number of markers (calbindin and parvalbumin), it remains possible that the overall number of amacrine cells is unchanged in the *En2*$^{-/-}$ retina, while only the gene expression profile of specific subtypes is altered.

Impaired scotopic ERG response in *En2*$^{-/-}$ adult mice

Molecular and structural alteration in photoreceptors and other cell types were accompanied by functional defects in the adult *En2*$^{-/-}$ retina. Specifically, scotopic ERG revealed a significant reduction of both a-wave and b-wave amplitude in *En2*$^{-/-}$ mice, as compared to controls (Fig. 7). To verify the level of visual defect in *En2*$^{-/-}$ mice, we calculated the b-wave/a-wave ratio at maximal flash intensity (Piano et al., 2016) in both genotypes. The values obtained in the two groups of animals were almost superimposable, indicating that the b-wave reduction recorded in *En2*$^{-/-}$ mice is proportional and related to the a-wave reduction. This suggests that the visual defect present in the En2$^{-/-}$ retina primarily resides at the level of rod photoreceptors and is amplified during the passage of the visual signal to bipolar cells. Photopic ERG responses were instead unchanged in *En2*$^{-/-}$ mice (Fig. 8). These results clearly

show that the deletion of the *En2* gene significantly affects rod (scotopic response) but not cone (photopic response) function. These electrophysiological results are in agreement with our expression data, showing a downregulation of rhodopsin mRNA and protein dimer (Fig. 2), as well as *Pcp2* mRNA (Fig. 4) in the mutant retina. Interestingly, a recent study revealed that rhodopsin dimerization is essential for the correct folding, maturation, and targeting of rhodopsin (Zhang et al., 2016), suggesting that physiological function of rhodopsin-mediated phototransduction could be altered in the *En2*$^{-/-}$ retina due to impaired rhodospin dimerization. *Pcp2* is supposed to be expressed only in ON bipolar cells (Xu et al., 2008). Thus, altered *Pcp2* expression actually fits with the functional (ERG) defects observed in mutant mice.

Retinal defects and their relevance for aberrant visual processing in ASD

Several studies show altered sensory processing in ASD patients, including deficits of visual function (reviewed in Lavoie et al., 2014; Robertson and Baron-Cohen, 2017). At the level of the visual cortex, major alterations in visual processing associated to ASD include preference for high contrast, atypical perception of global motion and weaker binocular rivalry, accompanied by lower levels of GABA (Robertson and Baron-Cohen, 2017). As regarding retinal function, a couple of ERG studies have been performed in ASD patients, consistently showing markedly reduced b-wave amplitude in both scotopic (Ritvo et al., 1988; Realmuto et al., 1989) and photopic (Constable et al., 2016) conditions. These results suggest that this particular ERG anomaly may represent a risk biomarker for ASD; in this respect, studies performed on mice lacking ASD-associated genes may be informative. Mice lacking the *Fmr1* gene, a model for Fragile X Syndrome (the most common form of mental retardation with ASD features), display significantly decreased content of

rhodopsin and reduced scotopic ERG b-wave amplitude (Rossignol et al., 2014). This is in agreement with what observed in the *En2*$^{-/-}$ retina, suggesting that in both mutants impaired rhodopsin function might be at the origin of the impaired visual signal transmission between photoreceptors and the inner retina. A recent study showed that retinal molecular defects in *Fmr1* mutant mice are present before eye opening and are maintained throughout adulthood, leading to electrophysiological deficits in the absence of any underlying structural changes (Perche et al., 2018). Interestingly, *Fmr1* expression is down-regulated in the brain of *En2*$^{-/-}$ mice both at mRNA and protein level (Provenzano et al., 2015), and *En2* and *Fmr1* mutant brains share neuroanatomical abnormalities (Ellegood et al., 2015). Taken together, these studies suggest that retinal deficits may impact on visual sensory processing in mice lacking the ASD-associated genes *Fmr1* and *En2*. Indeed, previous studies showed that both *Fmr1* and *En2* mutant mice have impaired visual cortical function (Dölen et al., 2007; Allegra et al., 2014).

Conclusions

In this study, we showed for the first time that anatomical and functional defects are present in the retina of the *En2* ASD mouse model. Our findings are in agreement with similar results obtained in other mouse strains lacking ASD-associated genes. Future work will be needed to understand how the observed retinal defects contribute to altered vision in mouse models of ASD.

ACKNOWLEDGEMENTS

We thank the administrative and technical staff of CIBIO for excellent assistance. The authors declare no conflict of interest. This work was supported by the University of Trento (start-up grant to S.C. and Y.B.). Y.B., S.C. and G.P. are currently supported by the University of Trento 2018-2020 Strategic Project “Trentino Autism Initiative – TRAIN”.

REFERENCES

Ades SE, Sauer RT (1994), Differential DNA-binding specificity of the engrailed homeodomain: the role of residue 50. Biochemistry 33:9187-9194.

Allegra M, Genovesi S, Maggia M, Cenni MC, Zunino G, Sgadò P, Caleo M, Bozzi Y (2014), Altered GABAergic markers, increased binocularity and reduced plasticity in the visual cortex of engrailed-2 kcockout mice. Front Cell Neurosci 8:163. doi: 10.3389/fncel.2014.00163.

Benayed R, Gharani N, Rossman I, Mancuso V, Lazar G, Kamdar S, Bruse SE, Tischfield S, et al. (2005), Support for the homebox transcription factor gene ENGRAILED2 as an autism spectrum disorder susceptibility locus. Am J Hum Genet 77:851-868.

Benayed R, Choi J, Matteson PG, Gharani N, Kamdar S, Brzustowicz LM, Millonig JH (2009), Autism-associated haplotype affects the regulation of the homeobox gene, Engrailed 2. Biol Psychiatry 66:911-917.doi:10.1016/j.biopsych.2009.05.027.

Behrmann M, Thomas C, Humphreys K (2006), Seeing it differently: visual processing in autism. Trends Cogn Sci 10:258-264.

Boschian C, Messina A, Bozza A, Castellini ME, Provenzano G, Bozzi Y, Casarosa S (2018), Impaired neuronal differentiation of neural stem cells lacking the Engrailed-2 gene. Neuroscience 386:137-149.

Brielmaier J, Matteson PG, Silverman JL, Senerth JM, Kelly S, Genestine M, Millonig JH, Dicicco-Bloom E, et al. (2012), Autism-relevant social abnormalities and cognitive deficits in Engrailed-2 knockout mice. PLoS ONE 7:e40914. doi: 10.1371/journal.pone.0040914.

Brunet I, Weinl C, Piper M, Trembleau A, Volovitch M, Harris W, Prochiantz A, Holt C (2005), The transcription factor Engrailed-2 guides retinal axons. Nature 438:94-98.

Chaya T, Matsumoto A, Sugita Y, Watanabe S, Kuwahara R, Tachibana M, Furukawa T (2017), Versatile functional roles of horizontal cells in the retinal circuit. Sci Rep 7:5540. doi: 10.1038/s41598-017-05543-2.

Cheh MA, Millonig JH, Roselli LM, Ming X, Jacobsen E, Kamdar S, Wagner GC (2006), En2 knock out mice display neurobehavioral and neurochemical alterations relevant to autism spectrum disorder. Brain Res, 1116:166-176.

Choi J, Ababon MR, Soliman M, Lin Y, Brzustowicz LM, Matteson PG, Millonig, JH (2014), Autism associated gene, engrailed2, and flanking gene levels are altered in post-mortem cerebellum. PLoS One 9:e87208. doi:10.1371/journal.pone.0087208.

Constable PA, Gaigg SB, Bowler DM, Jägle H, Thompson DA (2016), Full-field electroretinogram in autism spectrum disorder. Doc Ophthalmol 132:83-99.

Dakin S, Frith U (2005), Vagaries of visual perception in autism. Neuron 48:497-507.

Dölen G, Osterweil E, Rao BS, Smith GB, Auerbach BD, Chattarji S, Bear MF (2007), Correction of fragile X syndrome in mice. Neuron 56:955-962.

Ellegood J, Anagnostou E, Babineau BA, Crawley JN, Lin L, Genestine M, DiCicco-Bloom E, Lai JK, Foster JA, Peñagarikano O, Geschwind DH, Pacey LK, Hampson DR, Laliberté CL, Mills AA, Tam E, Osborne LR, Kouser M, Espinosa-Becerra F, Xuan Z, Powell CM, Raznahan A, Robins DM, Nakai N, Nakatani J, Takumi T, van Eede MC, Kerr TM, Muller C, Blakely RD, Veenstra-VanderWeele J, Henkelman RM, Lerch JP (2015), Clustering autism: using neuroanatomical differences in 26 mouse models to gain insight into the heterogeneity. Mol Psychiatry 20:118-125.

Freund CL, Gregory-Evans CY, Furukawa T, Papaioannou M, Looser J, Ploder L, Bellingham J, Ng D, Herbrick JA, Duncan A, Scherer SW, Tsui LC, Loutradis-Anagnostou A, Jacobson SG, Cepko CL,

Bhattacharya SS, McInnes RR (1997), Cone-rod dystrophy due to mutations in a novel photoreceptor-specific homeobox gene (CRX) essential for maintenance of the photoreceptor. Cell 91:543-553.

Furukawa T, Morrow EM, Cepko CL (1997), Crx, a novel otx-like homeobox gene, shows photoreceptor-specific expression and regulates photoreceptor differentiation. Cell 91:531-541.

Gharani N, Benayed R, Mancuso V, Brzustowics LM, Millonig JH (2004), Association of the homebox transcription factor, ENGRAILED2,3, with autism spectrum disorder. Mol Psychiatry 9:474-484.

Gherbassi D, Simon HH (2006), The engrailed transcription factors and the mesencephalic dopaminergic neurons. J Neural Transm Suppl 70:47–55.

Hancock HA, Kraft TW (2004), Oscillatory potential analysis and ERGs of normal and diabetic rats. Invest Ophth Vis Sci 45:1002–1008.

Happé F, Frith U (2006), The weak coherence account: detail-focused cognitive style in autism spectrum disorders. J Autism Dev Disord 36:5-25.

Haverkamp S, Wässle H (2000), Immunocytochemical analysis of the mouse retina. J Comp Neurol 424:1-23.

Haverkamp S, Ghosh KK, Hirano AA, Wässle H (2003), Immunocytochemical description of five bipolar cell types of the mouse retina. J Comp Neurol 455:463-476.

Hnoonual A, Sripo T, Limprasert P (2016), Whole-exome sequencing identifies a novel heterozygous missense variant of the EN2 gene in two unrelated patients with autism spectrum disorder. Psychiatr Genet 26:297-301.

Hughes AE, Enright JM, Myers CA, Shen SQ, Corbo JC (2017) Cell type-specific epigenomic analysis reveals a uniquely closed chromatin architecture in mouse rod photoreceptors. Sci Rep 7:43184. doi: 10.1038/srep43184.

James SJ, Shpyleva S, Melnyk S, Pavliv O, Pogribny IP (2013), Complex epigenetic regulation of engrailed-2 (EN-2) homeobox gene in the autism cerebellum. Transl Psychiatry 3:e232. doi: 10.1038/tp.2013.8.

James SJ, Shpyleva S, Melnyk S, Pavliv O, Pogribny IP (2014), Elevated 5-hydroxymethylcytosine in the Engrailed-2 (EN-2) promoter is associated with increased gene expression and decreased MeCP2 binding in autism cerebellum. Transl Psychiatry 4:e460. doi: 10.1038/tp.2014.87.

Jeon CJ, Strettoi E, Masland RH (1998), The major cell populations of the mouse retina. J Neurosci 18:8936-8946.

Joyner AL (1996), Engrailed, Wnt and Pax genes regulate midbrain—hindbrain development. Trends Genet 12:15-20.

Joyner AL, Herrup K, Auerbach BA, Davis CA, Rossant J (1991), Subtle cerebellar phenotype in mice homozygous for a targeted deletion of the En-2 homebox. Science 251:1239-1343.

Kim JW, Yang HJ, Oel AP, Brooks MJ, Jia L, Plachetzki DC, Li W, Allison WT, Swaroop A (2016), Recruitment of rod photoreceptors from short-wavelength-sensitive cones during the evolution of nocturnal vision in mammals. Dev Cell 37:520-532.

Koulen P, Fletcher EL, Craven SE, Bredt DS, Wässle H (1998), Immunocytochemical localization of the postsynaptic density protein PSD-95 in the mammalian retina. J Neurosci 18:10136-10149.

Kuemerle B, Zanjani H, Joyner A, Herrup K (1997), Pattern deformities and cell Loss in Engrailed-2 mutant mice suggest two separate patterning events during cerebellar development. J Neurosci 17:7881–7889.

Lavoie J, Maziade M, Hébert M (2014), The brain through the retina: the flash electroretinogram as a

tool to investigate psychiatric disorders. Prog Neuropsychopharmacol Biol Psychiatry 48:129-34. doi: 10.1016/j.pnpbp.2013.09.020.

Lei B, Yao G, Zhang K, Hofeldt KJ, Chang B (2006), Study of rod- and cone-driven oscillatory potentials in mice. Invest Ophth Vis Sci 47, 2732–2738.

Mitchell CK, Rowe-Rendleman CL, Ashraf S, Redburn DA (1995), Calbindin immunoreactivity of horizontal cells in the developing rabbit retina. Exp Eye Res 61:691-698.

Mo A, Luo C, Davis FP, Mukamel EA, Henry GL, Nery JR, Urich MA, Picard S, Lister R, Eddy SR, Beer MA, Ecker JR, Nathans J (2016), Epigenomic landscapes of retinal rods and cones. Elife 5:e11613. doi: 10.7554/eLife.11613.

Mottron L, Dawson M, Soulières I, Hubert B, Burack J (2006), Enhanced perceptual functioning in autism: an update, and eight principles of autistic perception. J Autism Dev Disord 36:27-43.

Perche O, Felgerolle C, Ardourel M, Bazinet A, Pâris A, Rossignol R, Meyer-Dilhet G, Mausset-Bonnefont AL, Hébert B, Laurenceau D, Montécot-Dubourg C, Menuet A, Bizot JC, Pichon J, Ranchon-Cole I, Briault S (2018), Early retinal defects in Fmr1(-/y) mice: toward a critical role of visual dys-sensitivity in the fragile X syndrome phenotype? Front Cell Neurosci 12:96. doi: 10.3389/fncel.2018.00096.

Piano I, Novelli E, Della Santina L, Strettoi E, Cervetto L, Gargini C. (2016), Involvement of autophagic pathway in the progression of retinal degeneration in a mouse model of diabetes. Front Cell Neurosci: 10:42. doi: 10.3389/fncel.2016.00042.

Provenzano G, Pangrazzi L, Poli A, Pernigo M, Sgadò P, Genovesi S, Zunino G, Berardi N, et al. (2014a), Hippocampal dysregulation of neurofibromin-dependent pathways is associated with impaired spatial learning in engrailed 2 knock-out mice. J Neurosci 34:13281-13288.

Provenzano G, Sgadò P, Genovesi S, Zunino G, Casarosa S, Bozzi Y. (2015), Hippocampal dysregulation of FMRP/mGluR5 signaling in Engrailed-2 knockout mice, a model of autism spectrum disorders. Neuroreport 26:1101-1105.

Realmuto G, Purple R, Knobloch W, Ritvo E (1989), Electroretinograms (ERGs) in four autistic probands and six first-degree relatives. Can J Psychiatry 34:435-439.

Ritvo ER, Creel D, Realmuto G, Crandall AS, Freeman BJ, Bateman JB, Barr R, Pingree C, Coleman M, Purple R (1988), Electroretinograms in autism: a pilot study of b-wave amplitudes. Am J Psychiatry 145:229-232.

Robertson CE, Baron-Cohen S (2017), Sensory perception in autism. Nat Rev Neurosci 18:671-684.

Rossignol R, Ranchon-Cole I, Pâris A, Herzine A, Perche A, Laurenceau D, Bertrand P, Cercy C, Pichon J, Mortaud S, Briault S, Menuet A, Perche O (2014), Visual sensorial impairments in neurodevelopmental disorders: evidence for a retinal phenotype in Fragile X Syndrome. PLoS One. 9(8):e105996. doi: 10.1371/journal.pone.0105996.

Sgadò P, Genovesi S, Kalinovsky A, Zunino G, Macchi F, Allegra M, Murenu E, Provenzano G, et al. (2013b), Loss of GABAergic neurons in the hippocampus and cerebral cortex of Engrailed-2 null mutant mice: implications for autism spectrum disorders. Exp Neurol 247:496-505.

Siegert S, Cabuy E, Scherf BG, Kohler H, Panda S, Le YZ, Fehling HJ, Gaidatzis D, Stadler MB, Roska B (2012), Transcriptional code and disease map for adult retinal cell types. Nat Neurosci 15:487-495.

Soltani A, Lebrun S, Carpentier G, Zunino G, Chantepie S, Maïza A, Bozzi Y, Desnos C, Darchen F, Stettler O (2017), Increased signaling by the autism-related Engrailed-2 protein enhances dendritic branching and spine density, alters synaptic structural matching, and exaggerates protein synthesis. PLoS One12(8):e0181350. doi: 10.1371/journal.pone.0181350.

Sudarov A, Joyner AL (2007), Cerebellum morphogenesis: the foliation pattern is orchestrated by multi-cellular anchoring centers. Neural Dev 2:26.

Thoreson WB, Mangel SC (2012), Lateral interactions in the outer retina. Prog Retin Eye Res 31:407-441.

Tripathi PP, Sgadò P, Scali M, Viaggi C, Casarosa S, Simon HH, Vaglini F, Corsini GU, et al. (2009), Increased susceptibility to kainic acid-induced seizures in Engrailed-2 knockout mice. Neuroscience 159: 842-849. doi:10.1016/j.neuroscience.2009.01.007.

Vlamings PH, Jonkman LM, van Daalen E, van der Gaag RJ, Kemner C (2010), Basic abnormalities in visual processing affect face processing at an early age in autism spectrum disorder. Biol Psychiatry 68:1107-1113.

Wizenmann A, Brunet I, Lam J, Sonnier L, Beurdeley M, Zarbalis K, Weisenhorn-Vogt D, Weinl C, Dwivedy A, Joliot A, Wurst W, Holt C, Prochiantz A (2009), Extracellular Engrailed participates in the topographic guidance of retinal axons in vivo. Neuron 64:355-366.

Wizenmann A, Stettler O, Moya KL (2015), Engrailed homeoproteins in visual system development. Cell Mol Life Sci 72:1433-1445.

Xu Y, Sulaiman P, Feddersen RM, Liu J, Smith RG, Vardi N (2008), Retinal ON bipolar cells express a new PCP2 splice variant that accelerates the light response. J Neurosci 28:8873-8884.

Zhang T, Cao LH, Kumar S, Enemchukwu NO, Zhang N, Lambert A, Zhao X, Jones A, Wang S, Dennis EM, Fnu A, Ham S, Rainier J, Yau KW, Fu Y (2016), Dimerization of visual pigments in vivo. Proc Natl Acad Sci U S A 113:9093-9098.

FIGURE LEGENDS

Figure 1. ***En2* mRNA is expressed in the adult mouse retina.** A) RT-PCR amplification of *En2* mRNA from *En2*$^{+/+}$ but not *En2*$^{-/-}$ adult mice retina. B) RT-PCR amplification of *En2* mRNA from the outer nuclear layer (ONL), inner nuclear layer (INL), and ganglion cell layer (GCL) collected by laser-capture microdissection of the adult *En2*$^{+/+}$ retina. C), Representative *in situ* hybridization confirming that *En2* mRNA is expressed in the ONL, INL, and GCL of the *En2*$^{+/+}$ but not *En2*$^{-/-}$ adult retina. D) Representative immunostaining showing that En2 protein (red) is expressed in the INL and GCL of the *En2*$^{+/+}$ adult retina. Abbreviations: ONL, outer nuclear layer; INL, inner nuclear layer; GCL, ganglion cells layer. OPL, outer plexiform layer; IPL, inner plexiform layer. Scale bar: 150 μm (C), 100 μm (D).

Figure 2. Rhodopsin expression is reduced in the retina of *En2*$^{-/-}$ adult mice. A) Representative rhodopsin immunohistochemistry (red) on retinal sections from *En2*$^{+/+}$ and *En2*$^{-/-}$ adult mice. Abbreviations: Rho, rhodopsin; ROS, rod outer segment. Scale bar: 25 μm. B) mRNA expression level of rhodopsin, as obtained by qRT-PCR performed on whole retinas of *En2*$^{+/+}$ and *En2*$^{-/-}$ adult mice. Values (box and whiskers plot, median with maximum/minimum) are expressed as rhodopsin/β-actin comparative quantitation ratios (*$p<0.05$, Mann-Whitney U test, *En2*$^{+/+}$ vs. *En2*$^{-/-}$, 3 mice per genotype). C) Rhodopsin immunoblottings from adult mouse retinas of both genotypes; three samples per genotype are shown. Rhodopsin oligomers (Rho olig), dimers (Rho dimer), and monomers (Rho mono) are shown. Glyceraldehyde 3-phosphate dehydrogenase (GAPDH) was used as internal standard; molecular weights (kDa) are indicated on the right. D) Quantification of rhodopsin immunoblotting experiments; rhodopsin dimer levels were normalized to GAPDH (box and whiskers plot, median with maximum/minimum; **$p<0.01$, Mann-Whitney U

test, *En2*$^{+/+}$ vs. *En2*$^{-/-}$, 3 mice per genotype).

Figure 3. Expression of cone photoreceptor markers in the adult retina of *En2*$^{+/+}$ and *En2*$^{-/-}$ adult mice. A) Representative immunostainings showing cone arrestin+ photoreceptors in the retina of *En2*$^{+/+}$ and *En2*$^{-/-}$ adult mice. Abbreviations: OS, outer segment; IS, inner segment; SE, synaptic endings. Scale bar: 25 μm. B) mRNA expression levels of S- and M-opsin, as obtained by qRT-PCR performed on whole retinas of *En2*$^{+/+}$ and *En2*$^{-/-}$ adult mice. Values (box and whiskers plot, median with maximum/minimum) are expressed as each marker/β actin comparative quantitation ratios (3 mice per genotype). C) (Top) S- and M-opsin immunoblottings from adult mouse retinas of both genotypes; three samples per genotype are shown. GAPDH was used as internal standard. (Bottom) Quantification of S- and M-opsin immunoblotting experiments; opsin levels were normalized to GAPDH (box and whiskers plot, median with maximum/minimum; 3 mice per genotype). D) Representative immunostainings showing PSD-95 labelled photoreceptor synaptic terminals (green) in the retina of *En2*$^{+/+}$ and *En2*$^{-/-}$ adult mice. SE, synaptic endings. Scale bar: 50 μm.

Figure 4. Expression of bipolar cell markers in the adult retina of *En2*$^{+/+}$ and *En2*$^{-/-}$ adult mice. A) *Pcp2* mRNA is downregulated in the *En2*$^{-/-}$ retina. mRNA expression was measured by qRT-PCR on whole retinas of *En2*$^{+/+}$ and *En2*$^{-/-}$ adult mice. Values (box and whiskers plot, median with maximum/minimum) are expressed as *Pcp2*/β actin comparative quantitation ratios (***$p<0.001$, Mann-Whitney U test, *En2*$^{+/+}$ vs. *En2*$^{-/-}$, 3 mice per genotype). B) Representative immunostainings showing PKCα-labelled bipolar cells (green) in the retina of *En2*$^{+/+}$ and *En2*$^{-/-}$ adult mice. Scale bar: 25 μm.

Figure 5. Expression of horizontal, amacrine, and ganglion cell markers in the adult retina of *En2*$^{+/+}$ and *En2*$^{-/-}$ adult mice. A, C, E) Representative pictures showing calbindin^{+} horizontal cells (A), calbindin^{+} amacrine/ganglion cells (C), and Brn3a+ ganglion cells (E) in the retina of adult mice from both genotypes. Positive cells are labeled in green. Scale bars: 50µm. B, D, F) Quantification of calbindin and Brn3a cell densities in *En2*$^{+/+}$ and *En2*$^{-/-}$ adult retinas. Values are expressed as labelled cells per mm^2 (box and whiskers plot, median with maximum/minimum; 3-4 mice per genotype; *p<0.05, Mann-Whitney U test, *En2*$^{+/+}$ vs. *En2*$^{-/-}$).

Figure 6. Expression of parvalbumin mRNA in the adult retina of *En2*$^{+/+}$ and *En2*$^{-/-}$ adult mice. Parvalbumin mRNA is upregulated in the *En2*$^{-/-}$ retina. mRNA expression was measured by qRT-PCR on whole retinas of *En2*$^{+/+}$ and *En2*$^{-/-}$ adult mice. Values (box and whiskers plot, median with maximum/minimum) are expressed as parvalbumin/β actin comparative quantitation ratios (**p<0.01, Mann-Whitney U test, *En2*$^{+/+}$ vs. *En2*$^{-/-}$, 3 mice per genotype).

Figure 7. Impairment of scotopic retinal function in *En2*$^{-/-}$ mice. (A) Representative scotopic flash ERG recordings from *En2*$^{+/+}$ and *En2*$^{-/-}$ mice in response to a flash intensity of 377.2 cd*s/m^2, the highest used for all experiments. (B, C) Scotopic a-wave and b-wave amplitude as a function of flash intensity from *En2*$^{+/+}$ and *En2*$^{-/-}$ mice. The traces show impaired ERG function in *En2*$^{-/-}$ mice: both a-wave and b-wave amplitude is significantly reduced. In (B), the graph shows only the luminance values at which the analysis of the 7ms a-wave was carried out (scotopic ERG protocol is normally carried out with a greater number of luminous intensities, see C). (D) Scotopic b-wave peak time (ms) as a function of flash intensity; the kinetics of ERG response is comparable between *En2*$^{+/+}$ and *En2*$^{-/-}$

mice. Note that the flash intensity scale reports only luminance values analyzed at peak time. (E, F) Scotopic OPs amplitude and kinetics, respectively**.** Values are expressed as mean ± s.e.m. (*p<0.05, **p<0.01, Tukey's test following two-way ANOVA, *En2*$^{+/+}$ vs. *En2*$^{-/-}$, 6 mice per genotype).

Figure 8. Preservation of photopic retinal function in *En2*$^{-/-}$ mice. (A) Representative photopic flash ERG recordings from *En2*$^{+/+}$ and *En2*$^{-/-}$ mice in response to a flash intensity of 377 cd*s/m^2 (the highest used for all experiments) superimposed on steady background of 30cd/m^2. (B) Photopic b-wave amplitude as a function of flash intensity from *En2*$^{+/+}$ and *En2*$^{-/-}$ mice. Traces show that cones function is preserved in *En2*$^{-/-}$ mice and the ERG amplitude is the comparable between *En2*$^{+/+}$ and *En2*$^{-/-}$ mice. The graph shows all the luminances used in the photopic ERG protocol, which are the medium and high intensity luminances also used in the scotopic ERG, but are imposed above a fixed background of 30cd/m^2. (C) Photopic b-wave peak time (ms) as a function of flash intensity; the kinetics of ERG response obtained from the cone-pathway is comparable between *En2*$^{+/+}$ and *En2*$^{-/-}$ mice. (D, E) Photopic oscillatory potentials (OP1-OP4) extracted from ERG response to the bright test flash (377cd*s/m^2). Both amplitude and kinetic functions show no difference between *En2*$^{+/+}$ and *En2*$^{-/-}$ mice. Values are expressed as mean ± s.e.m. (p>0.05, two-way ANOVA, *En2*$^{+/+}$ vs. *En2*$^{-/-}$, 6 mice per genotype).

TABLES

Gene name	Forward	Reverse
En1	5′-AGTGGCGGTGGTAGTGGA-3′	5′-CCTTCTCGTTCTTTTTCTTCTTT-3′
En2 (RT-PCR)	5′-ACTGCACGCGCTATTCTG-3′	5′-ACCTGTTGGTCTGAAACTCAG-3′
En2 (ISH)	5′-GCGTAATACGACTCACTATAGGGAAAGGGGACTCTTTAGGGTTTC-3′	5′-CGCATTAACCCTCACTAAAGGGAGAAGATGATTCCAACTCGCTCT-3′
Rhodopsin	5′-GCCTGAGGTCAACAACGAAT-3′	5′-GATAACCATGCGGGTGACTT-3′
M-opsin	5′-CTCTGCTACCTCCAAGTGTGG-3′	5′-AAGGTATAGGGTCCCCAGCAGA-3′
S-opsin	5′-TGTACATGGTCAACAATCGGA-3′	5′-ACACCATCTCCAGAATGCAAG-3′
Pcp2	5′-AGGCTTCTTCAACCTGCAGA-3′	5′-CGTTTCTGCATTCCATCCTT-3′
Parvalbumin	5′-TGCTCATCCAAGTTGCAGG-3‘	5′-GCCACTTTTGTCTTTGTCCAG-3′
β-actin	5′-AATCGTGCGTGACATCAAAG-3′	5′-AAGGAAGGCTGGAAAAGAGC-3′

Table 1. Primers used for RT-PCR and *in situ* hybridization (ISH) experiments.

Antibodies	Use	Dilution	Producer/cat. #
Goat polyclonal anti-EN2	IHC	1:250	Abcam ab45867
Mouse monoclonal anti-rhodopsin	IHC, IB	1:5000	Sigma O4886
Mouse monoclonal anti-GAPDH	IB	1:5000	Santa Cruz sc-32233
Rabbit polyclonal anti-cone arrestin	IHC	1:2000	Millipore AB15282
Rabbit polyclonal anti S-opsin	IB	1:200	Millipore AB5407
Rabbit polyclonal anti M-opsin	IB	1:200	Millipore AB 5405
Mouse monoclonal anti PKC-α	IHC	1:200	Santa Cruz sc-8393
Rabbit monoclonal anti-PSD-95	IHC	1:200	Cell Signaling 3450S
Rabbit polyclonal anti-calbindin D-28k	IHC	1:5000	Swant CB38
Mouse monoclonal anti-Brn3a	IHC	1:500	Millipore MAB1585
Donkey anti-mouse Alexa 488	IHC	1:1000	Life Technologies A-21202
Goat anti-rabbit Alexa 488	IHC	1:1000	Life Technologies A11034
Goat anti-rabbit Alexa 594	IHC	1:1000	Life Technologies A11037
Bovine anti-goat Alexa 594	IHC	1:1000	Jackson ImmunoLab 805-585-1800

Table 2. Antibodies used for immunohistochemistry (IHC) and immunoblotting (IB) experiments.

Marker	Experiment	Direction of change ($En2^{-/-}$ vs. $En2^{+/+}$)
Rhodopsin mRNA	qRT-PCR	decreased
Rhodopsin protein dimer	IB	decreased
cone arrestin	IHC	no change
S opsin mRNA	qRT-PCR	no change
S opsin protein	IB	no change
M opsin mRNA	qRT-PCR	no change
M opsin protein	IB	no change
PSD-95	IHC	no change
Pcp2 mRNA	qRT-PCR	decreased
PKCα	IHC	no change
calbindin^{+} horizontal cells	IHC	decreased
calbindin^{+} amacrine/ganglion cells	IHC	no change
Brn3a^{+} ganglion cells	IHC	no change
parvalbumin mRNA	qRT-PCR	increased

Table 3. Summary of marker expression in *En2*$^{-/-}$ *vs. En2*$^{+/+}$ adult retinas. Abbreviations: IB, immunoblotting, IHC, immunohistochemistry; other abbreviations as in the text.

Figure 1
Click here to download high resolution image

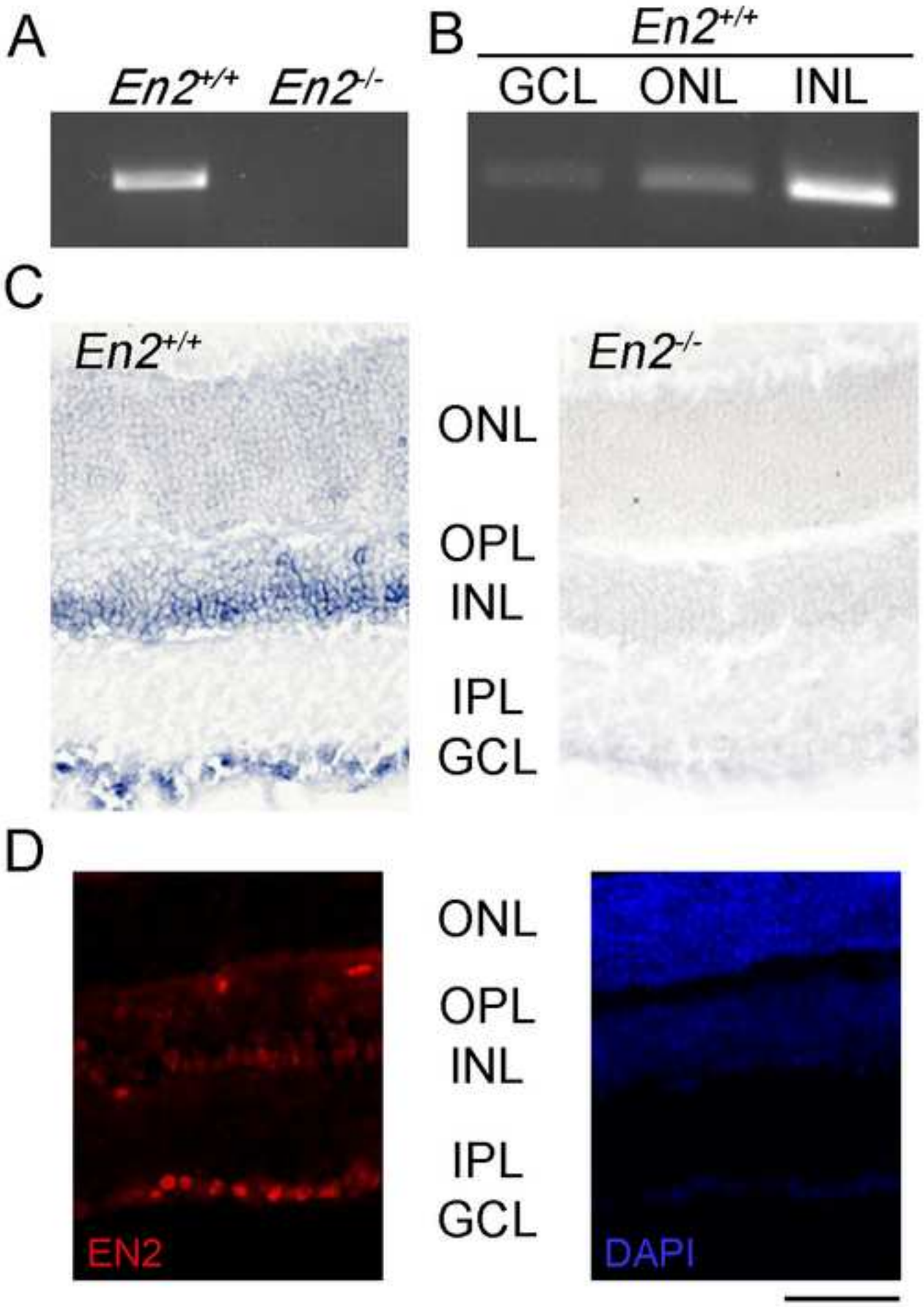

Figure 2
Click here to download high resolution image

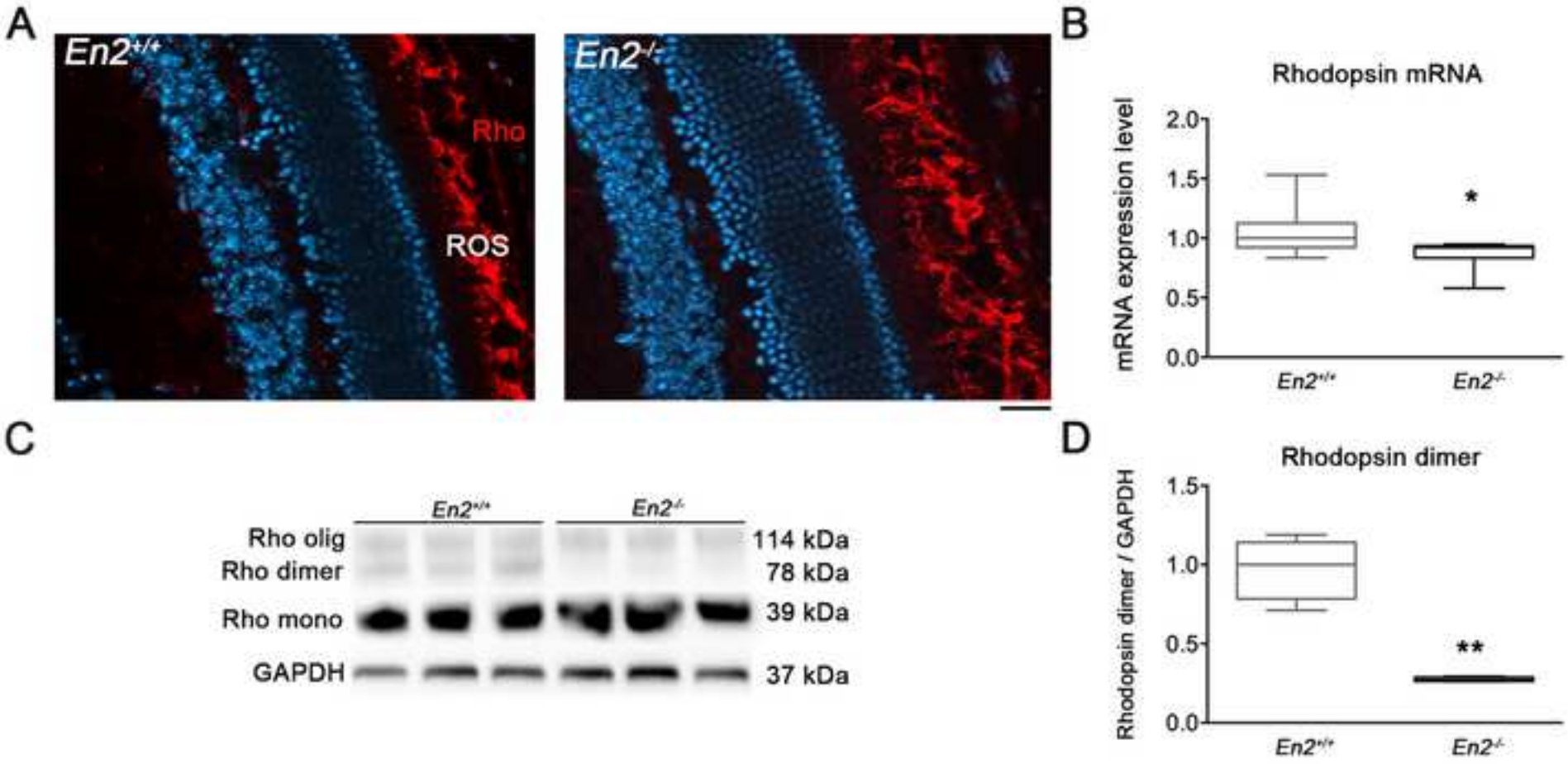

Figure 3
Click here to download high resolution image

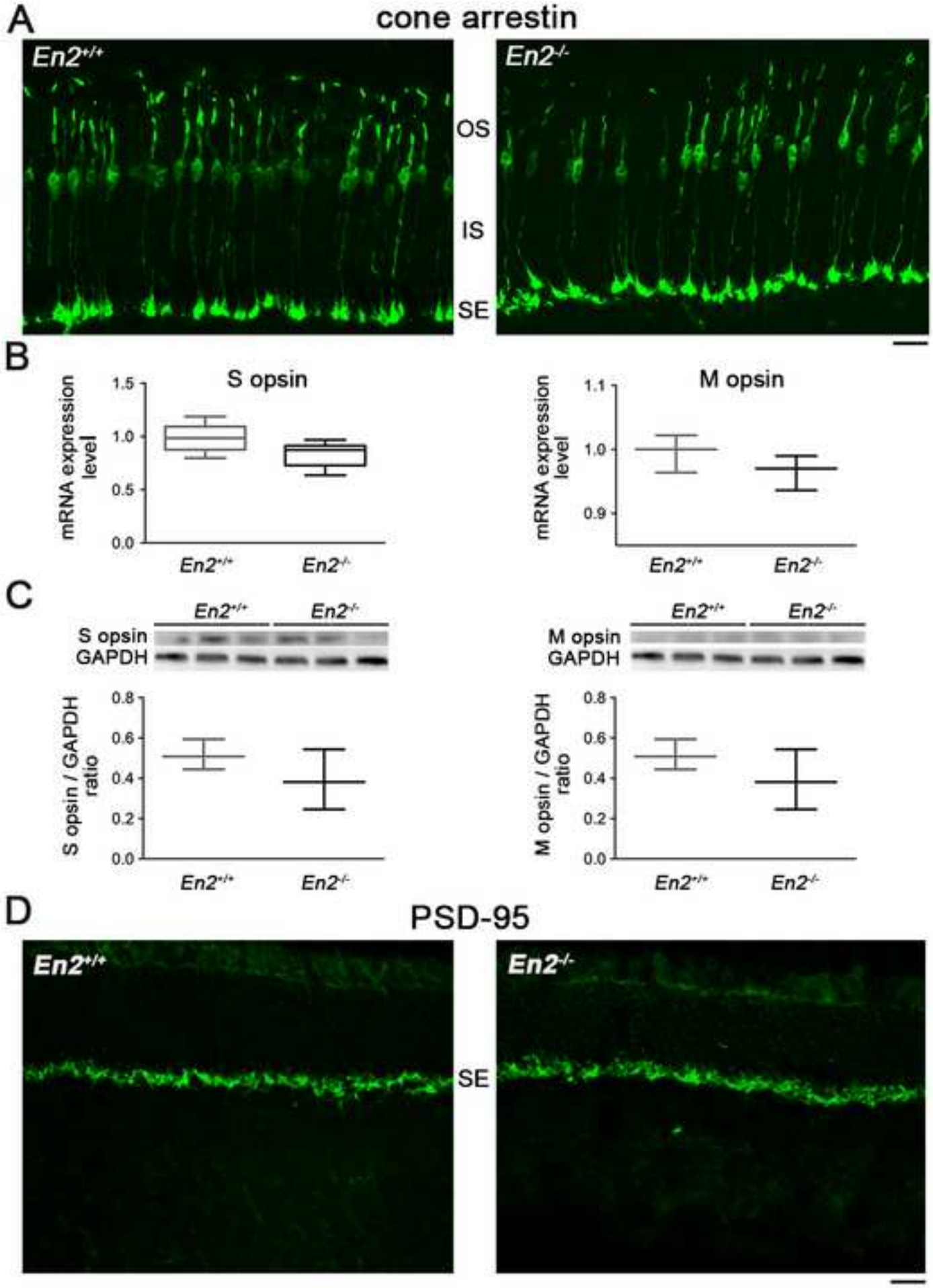

Figure 4
Click here to download high resolution image

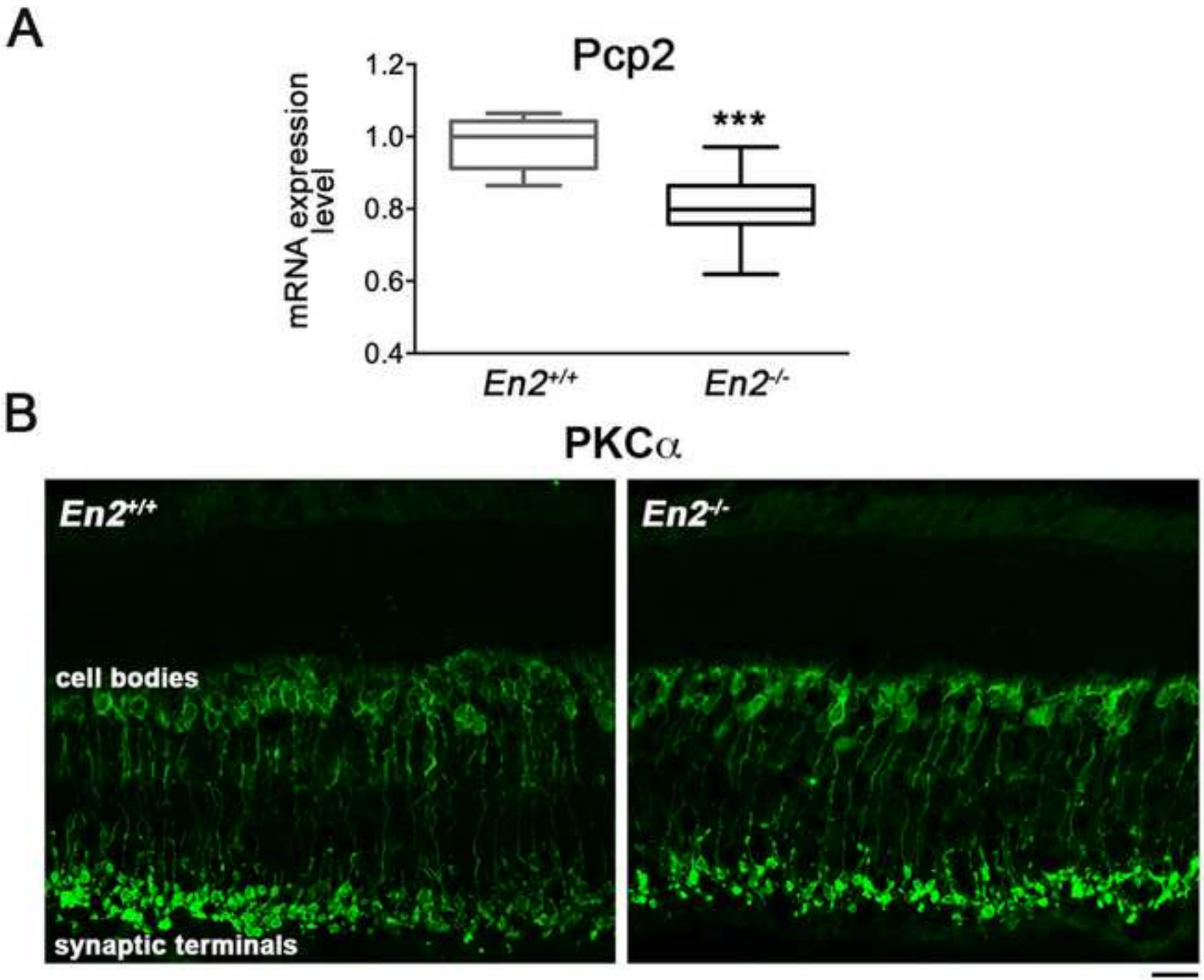

Figure 5
Click here to download high resolution image

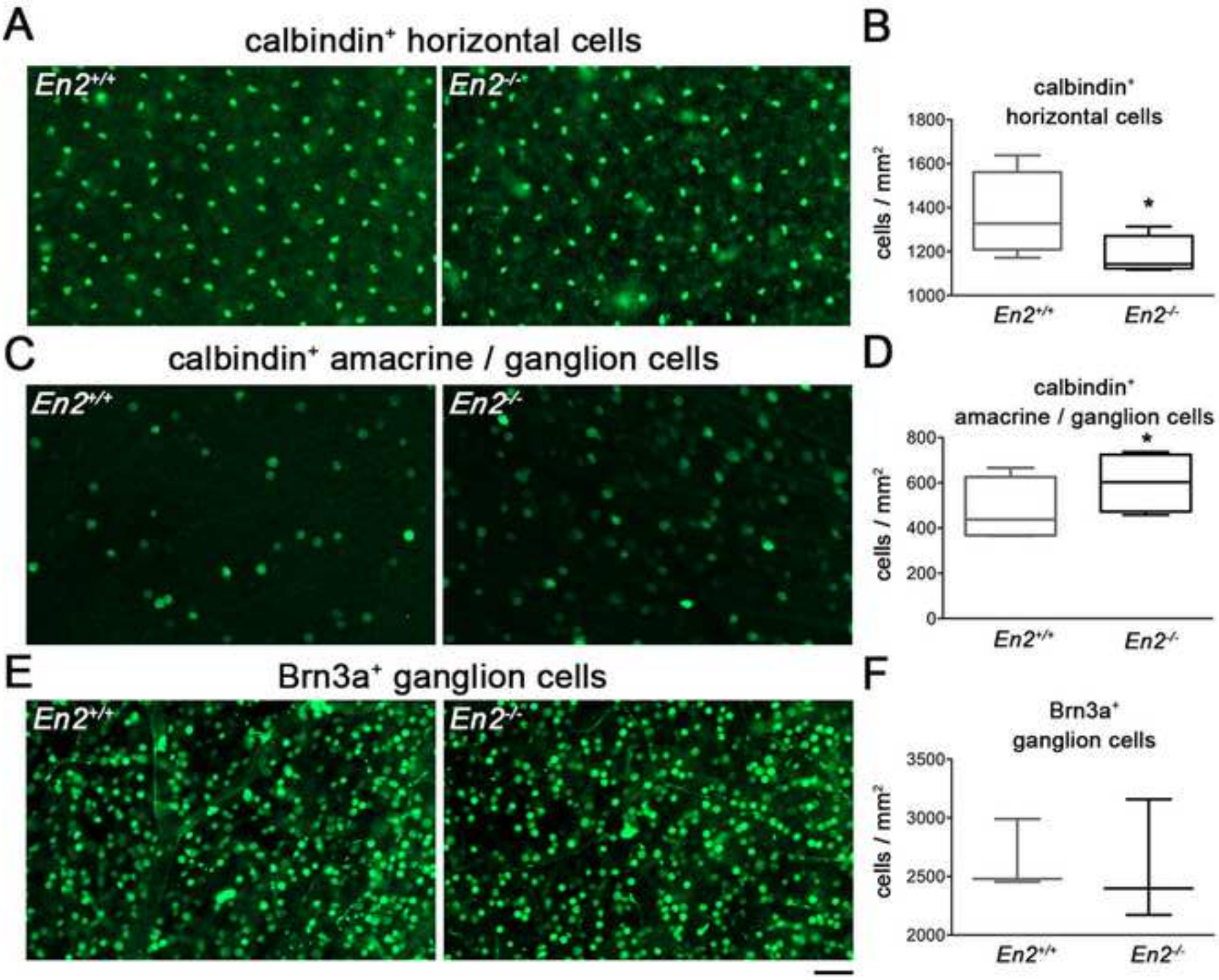

Figure 6
Click here to download high resolution image

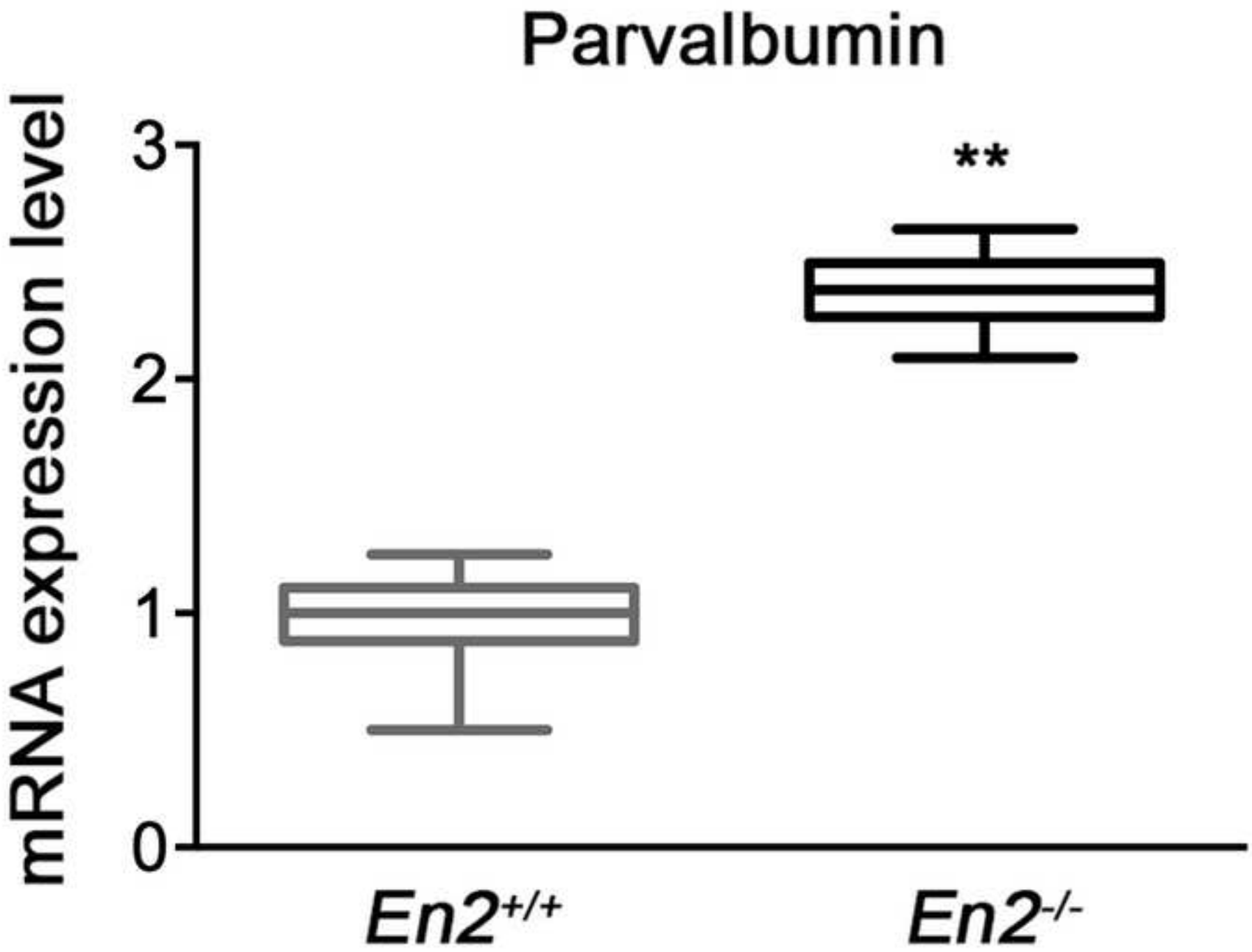

Figure 7
Click here to download high resolution image

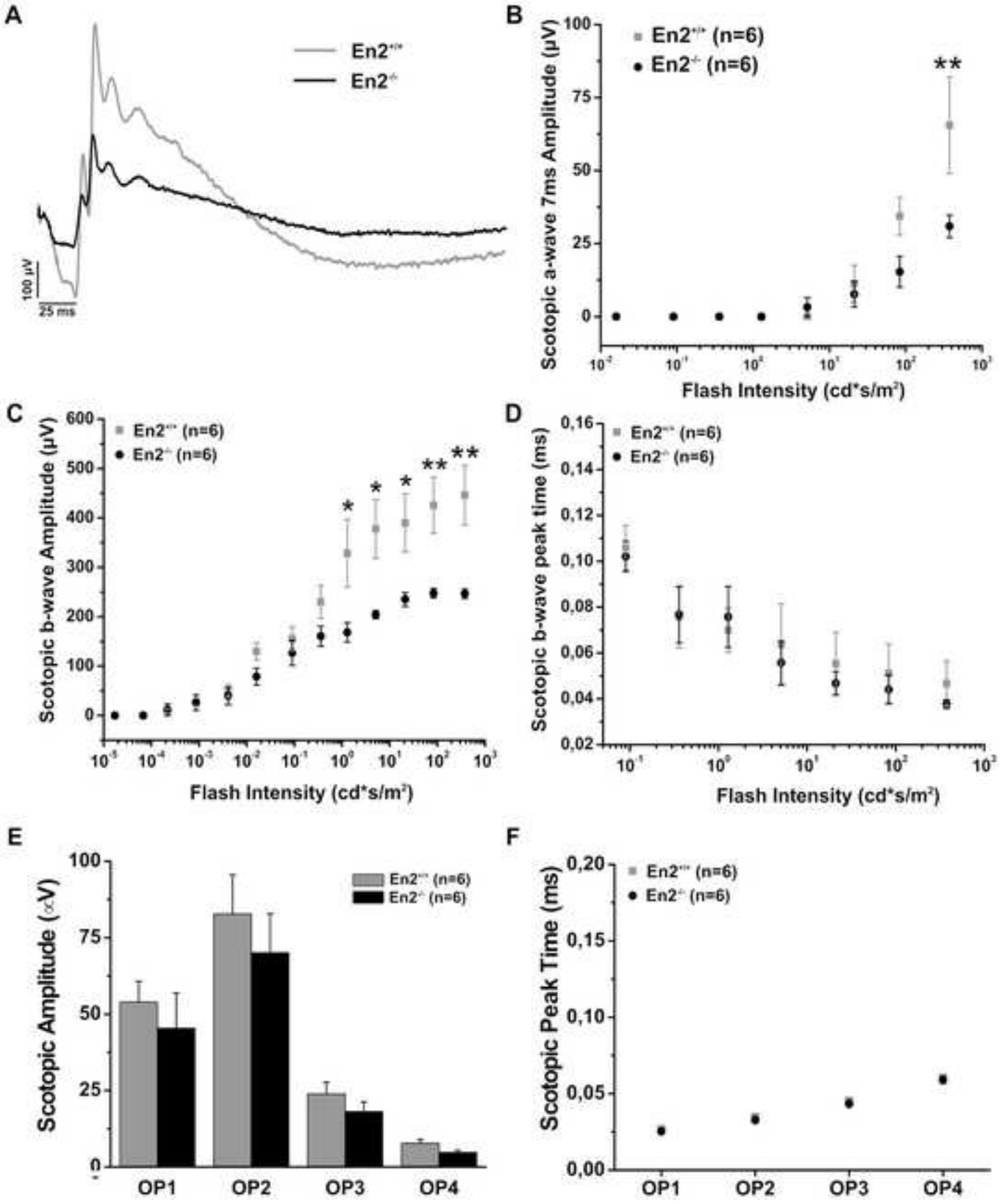

Figure 8

Click here to download high resolution image